Aminoindole and Naphthalimide based Charge Transfer Fluorescent Probes for pH Sensing and Live Cell Imaging

Sushil Sharma, Sai Srinivas, Sabyasachi Rakshit* and Sanchita Sengupta*

Department of Chemical Sciences, Indian Institute of Science Education and Research (IISER) Mohali, Knowledge City, Sector 81, P.O. Manauli, Mohali, Punjab 140306, India.

*E-mail: sanchita@iisermohali.ac.in, srakshit@iisermohali.ac.in

Table of contents

1. Materials and Methods:

All chemicals and solvents were purchased from commercial suppliers (Sigma Aldrich, SD Fine Chemicals) and used without further purification. Toluene (Tol) was dried over sodium/benzophenone and distilled prior to use. *N*, *N*-dimethylformamide (DMF) was dried over calcium hydride and distilled prior to use. Silica gel of mesh size 60-120 was used for column chromatography. The ^{1}H and ^{13}C NMR spectra were recorded on a 400 MHz Bruker Biospin Avance III FT-NMR spectrometer, respectively with TMS as standard at room temperature. The solvent used was $CDCl_3$ (from Merck, Germany) and all the spectra were recorded in $CDCl_3$ and dimethyl sulfoxide-d_6 (DMSO) with TMS as the internal standard. Mass spectrometry measurements were performed on UltrafleXtreme MALDI TOF/TOF (Bruker Daltonics) instrument. Software used for acquiring mass spectra was Flex Control, Bruker (USA) and software used for analyzing mass spectra was Flex Analysis 3.1.

All spectroscopic measurements were performed at room temperature unless otherwise mentioned. UV/Vis spectra were recorded on Carey 5000 UV/Vis spectrophotometer using a quartz cuvette with 1 cm path length. Fluorescence solution measurements were performed with Hitachi F7000 fluorescence spectrophotometer equipped with R928F photomultiplier expandable up to 900 nm. Various excitation wavelengths were used to perform the fluorescence measurements. Standard software FL Solutions was used for the measurement and analysis of the data.

Electrochemical measurements were performed using CHI-610E electrochemical workstation from CH Instruments (USA), with a conventional three electrode single-compartment cell consisting of a glassy carbon as the working electrode, Ag/AgCl containing 3M KCl solution as the reference electrode, and Pt wire as the counter electrode. Cyclic voltammetry measurements were performed at a scan-rate of 0.1 V/s. As a supporting electrolyte, 0.1 M tetrabutylammonium hexafluorophosphate (TBAHPF) (Alfa Aesar)

dissolved in pre-dried DCM was used. The solutions were purged with nitrogen for 2 mins prior to measurement. The concentration of the prepared samples was ~ 0.1-0.3 mM. The electrochemical potential was internally calibrated against the standard ferrocene/ferrocenium (Fc/Fc^+) redox couple.

Temperature-dependent fluorescence of samples were measured using temperature-controlled cuvette holder for Hitachi F7000 spectrophotometer (Luma 40) from Quantum Northwest. The Luma 40 was used for temperature range of -20 ^oC to +100 ^oC.

Temperature-dependent UV/Vis measurements were performed by Cary 300 spectrophotometer equipped with a dual cell peltier temperature controller with operating temperatures of 0 ^oC to 100 ^oC.

Time resolved fluorescence spectra were measured using time correlated single photon counting (TCSPC) model from Fluorocube, Horiba Jobin Yvon, NJ equipped with picosecond laser diodes as excitation source. The 375 nm laser diode was used as a light source for the excitation of samples and the instrument response function (IRF) was collected using Ludox (colloidal silica) solution. The width (FWHM) of IRF was ~ 250 ps. The optical pulse durations from < 70ps were used. Highly integrated picosecond PMT modules as well as micro channel plate PMTs were used for the time resolution.

Quantum chemical density functional theory (DFT) calculations were performed for **AIN**, **AINP** and **F-AINP** in ground state using Gaussian09 program suite.[S1] The side chains in all molecules were replaced with methyl group in order to account for the electron donating effect of the alkyl chain and at the same time reducing the computational time and cost. The studied molecules were optimized using global hybrid B3LYP functional and 6–31G (d, p) basis set in gas phase. The frontier molecular orbitals (FMO) electronic levels and FMO distribution were obtained from geometry optimization into neutral ground state geometries.

Cell Viability Assay

MTT (3-(4,5-dimethylthiazol-2-yl)-2,5-diphenyl-tetrazolium bromide) (TC191, Himedia) assay was performed to measure the viability of A549 cells treated with **AINP** and **FAINP**. The assays were performed in triplicates with the cells seeded on a 96-well plate. The media was discarded from the cells, and 50 µl of MTT stock solution (5 mg/ml) was added to each well containing 50 µl of Opti-MEM media. After incubating the plate at 37 ºC for 3 hours, 150 µl of DMSO (MTT solvent) was added to each well and shaken for 15 minutes. The absorbance of the reaction mixture was measured at 590 nm using a microplate reader and analyzed the results.

Dye treatment to cells

The adherent lung cancer cell line A549 and the fibroblast cell line L929 were obtained from NCCS, Pune. The cells were cultured in high glucose DMEM media (D1152, Sigma-Aldrich) supplemented with 10% Fetal Bovine Serum (FBS) and maintained at 37 ºC and 5% CO_2. The cells grown for 50 % confluency were treated with 0.005 mg/mL of **AINP** and **FAINP** diluted in DMEM and incubated for 10 min at 37 ºC. Following the incubation, the media was removed, washed twice with 1X PBS solution, and added the fresh media. Wheat Germ Agglutinin (WGA) (5 µg/ml), Hoechst (1 µg/ml), and Lysotracker reagents (50 nM) were used to stain the membrane, nucleus, and lysozymes, respectively. The stained cells were imaged using a super-resolution microscope (Zeiss LSM980 Airyscan 2) at 63X magnification and an inverted microscope (Leica Dmi8) at 40X magnification. The fluorescence excitation/emission wavelength of dyes are as follows: $\lambda_{ex}/\lambda_{em}$ = 488/510 nm; WGA $\lambda_{ex}/\lambda_{em}$ = 595/615 nm; Hoechst $\lambda_{ex}/\lambda_{em}$ = 360/460 nm; Lysotracker $\lambda_{ex}/\lambda_{em}$ = 595/615 nm.

2. Synthesis

Synthesis of 1-Aminoindole (AI):

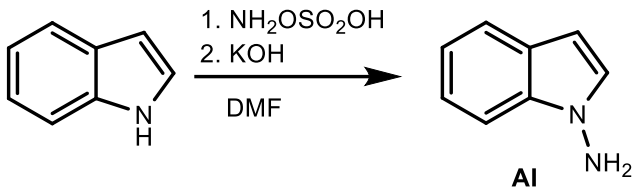

Scheme S1. Synthesis of 1-Aminoindole (AI).[S2]

Procedure: Crushed potassium hydroxide (KOH) (4.99 g, 88.94 mmol) was added in the solution of indole (500 mg, 4.27 mmol) in anhydrous DMF. Hydroxylamine O-Sulfonic acid (HOSA) (1.78 g, 15.75 mmol) was added portion wise (HOSA and DMF mixture) to this suspension solution and stirred for 4 h at room temperature. The reaction mixture was poured in cold water and extraction was performed by ethyl acetate. The organic layer was dried over Na_2SO_4 and evaporated under vacuum using rotary evaporator to give a crude product, which was purified by column chromatography on silica gel using ethyl acetate/hexane (1/9 v/v) as the eluent. The pure product was obtained as a brownish liquid with a yield of 37 %.

^{1}H NMR (400MHz, $CDCl_3$): δ (ppm) 7.60 (d, *J* = 8 Hz, 1 H), 7.37 (d, *J* = 8 Hz, 1 H), 7.23 (t, *J* = 8 Hz, 1 H), 7.11 (t, *J* = 8 Hz, 2 H), 6.37 (s, 1 H), 4.68 (s, 2 H).

Synthesis of 7-fluoroAminoindole (F-AI):

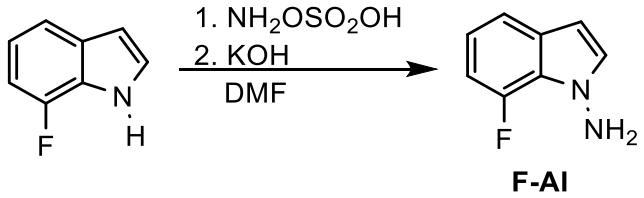

Scheme S2. Synthesis of 7-fluoroAminoindole (**F-AI**).[S2]

Procedure: Crushed potassium hydroxide (KOH) (4.32 g, 77.11 mmol) was added in the solution of indole (500 mg, 3.7 mmol) in anhydrous DMF. A solution of Hydroxylamine O-

sulfonic acid (HOSA) (1.54 g, 13.65 mmol) was added drop wise to this suspension and stirred for 4 h at room temperature. The reaction mixture was poured in cold water and extraction was performed by ethyl acetate. The organic layer was dried over Na_2SO_4 and evaporated under vacuum using rotary evaporator to give a crude product. The crude compound was further used without purification at this step.

Synthesis of 6-Bromo-2-(2,6-diisopropylphenyl)-1H-benzo[de]isoquinoline-1,3(2H)-dione (NP, 3):

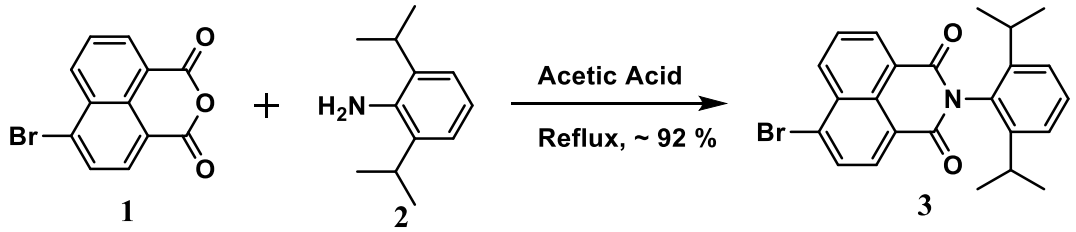

Scheme S3. Synthesis of 6-Bromo-2-(2,6-diisopropylphenyl)-1H-benzo[de]isoquinoline-1,3(2H)-dione (**NP**, **3**)[S3]

Procedure: To a solution of 6-bromo-1,8-napthalic anhydride (**1**) (500 mg, 1.8 mmol) in acetic acid (10 mL) in two neck round-bottomed flask, 2,6-diisopropylaniline (1.36 mL, 7.22 mmol) was added dropwise in nitrogen atmosphere and reflux for 5 h. The reaction mixture was cooled down and added in ice cold water and then formed precipitate was filtered, washed with water and dried. Compound **3** was purified by column chromatography using hexane/ethyl acetate (80/20, v/v) as the eluent. The pure product was obtained as a white solid with a yield of 92 %.

^{1}H NMR (400MHz, $CDCl_3$): δ (ppm) 8.73 (dd, J = 8 Hz, 1 H), 8.67 (dd, J = 8 Hz, 1 H), 8.49 (d, J = 8 Hz, 1 H), 8.10 (d, J = 8 Hz, 1 H), 7.91 (dd, J = 8 Hz, 1 H), 7.51 – 7.46 (t, J = 8 Hz, 1 H), 7.34 (s, 1 H), 7.32 (s, 1 H), 2.76 – 2.66 (m, 2 H), 1.15 (d, J = 8 Hz, 12 H).

Synthesis of 6-(1H-indole-1-y1)amino)-1H,3H-benzo[de]isochromene-1,3-dione (AIN):

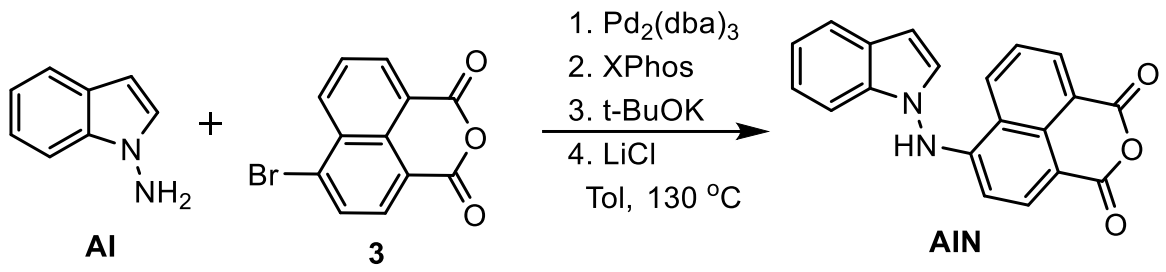

Scheme S4. Synthesis of 6-(1H-indole-1-y1)amino)-1H,3H-benzo[de]isochromene-1,3-dione (**AIN**).[S4]

Procedure: 1-Aminoindole (50 mg, 0.378 mmol) and 6-bromo-1,8-napthalic anhydride (105 mg, 0.378 mmol) were dissolved in toluene and degassed by freeze pump thaw method. In two neck round-bottomed flask, $Pd_2(dba)_3$ (2.5 mol%), XPhos (5 mol%), LiCl (32.04 mg, 0.756 mmol) and *t*-BuOK (63.62 mg, 0.567 mmol) were taken and simultaneously 1-Aminoindole and 6-bromo-1,8-napthalic anhydride were added and stirred for 4-5 h at 130 °C. The reaction mixture was cooled and filtered through celite pad using ethyl acetate and the final compound was purified by column chromatography using ethyl acetate and hexane (20:90 of ethyl acetate/hexane). The final compound was obtained as yellow solid with 45 % yield.

^{1}H NMR (400 MHz, DMSO-d_6): δ 11.24 (s, 1 H), 8.90 (d, *J* = 8 Hz, 1 H), 8.57 (d, *J* = 8 Hz, 1 H), 8.24 (d, *J* = 8 Hz, 1 H), 7.94 (m, 1 H), 7.71 (d, *J* = 4 Hz, 1 H), 7.63 (d, *J* = 8 Hz, 1 H), 7.23 (s, 1 H), 7.17 (s, 2 H), 6.72 (s, 1 H), 5.99 (d, *J* = 8.4 Hz, 1 H).

^{13}C NMR (101 MHz, DMSO-d_6): δ 161.90, 160.66, 151.39, 136.17, 135.18, 133.50, 131.97, 129.98, 129.35, 126.82, 126.62, 123.08, 121.67, 121.03, 119.46, 119.30, 109.51, 108.42, 105.97, 102.01.

ESI-TOF: $(M+H)^+$ of molecular formula $C_{20}H_{12}N_2O_3$: Calculated 329.0926; found 329.0941.

Synthesis of 6-((1H-indol-1-yl)amino)-2-(2,6-diisopropylphenyl)-1H-benzo[de]isoquinoline-1,3(2H)-dione (AINP):

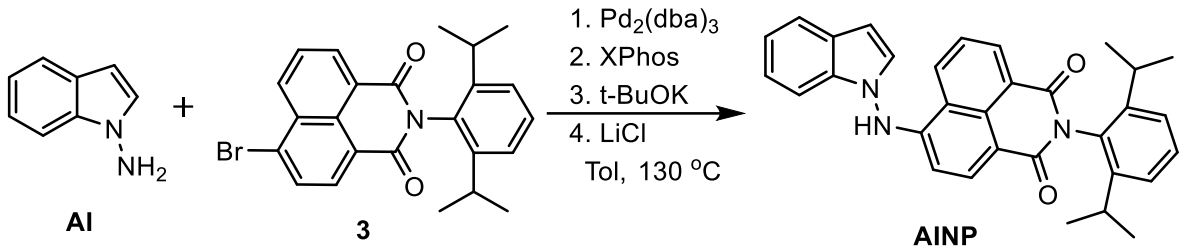

Scheme S5. Synthesis of 6-((1H-indol-1-yl)amino)-2-(2,6-diisopropylphenyl)-1H-benzo[de]isoquinoline-1,3(2H)-dione (**AINP**).[S4]

Procedure: 1-Aminoindole (37 mg, 0.276 mmol) and the compound **3** (100 mg, 0.23 mmol) were dissolved in toluene and degassed by freeze pump thaw method. In a two-neck round-bottomed flask, $Pd_2(dba)_3$ (2.5 mol%), XPhos (5 mol%), LiCl (20 mg, 0.46 mmol) and *t*-BuOK (39 mg, 0.345 mmol) were taken and simultaneously 1-Aminoindole and compound **3** were added and stirred for 4-5 h at 130 °C. The reaction mixture was cooled and filtered through celite pad using ethyl acetate and the final compound was purified by column chromatography using ethyl acetate and hexane (10:90, v/v) as eluent. The final compound was obtained as yellow solid with 40 % yield.

^{1}H NMR (400 MHz, DMSO): δ (ppm) 11.14 (s, 1 H), 8.92 (d, *J* = 8 Hz, 1 H), 8.62 (d, *J* = 6.4 Hz, 1 H), 8.27 (d, *J* = 8 Hz, 1 H), 7.94 (dd, *J* = 8, 8 Hz, 1 H), 7.70 (dd, *J* = 8 Hz, 1 H), 7.61 (d, *J* = 4 Hz, 1 H), 7.44 – 7.40 (m, 1 H), 7.31 – 7.26 (m, 3 H), 7.20 – 7.13 (m, 2 H), 6.71 (dd, *J* = 4 Hz, 1 H), 6.02 (d, *J* = 12 Hz, 1 H), 2.62 (m, 2 H), 1.04 (dd, *J* = 8, 4 Hz, 12 H).

^{13}C NMR (101 MHz, DMSO): δ (ppm) 163.94, 163.15, 150.48, 145.41, 134.83, 134.23, 131.82, 131.42, 129.54, 128.99, 128.92, 126.36, 126.03, 123.60, 122.55, 121.99, 121.18, 120.50, 119.14, 111.95, 109.16, 105.45, 101.41, 28.55, 23.61.

ESI-TOF: $(M+H)^+$ of molecular formula $C_{32}H_{29}N_3O_2$: Calculated 488.2338; found 488.2355.

In order to confirm the presence of N-H peak proton NMR spectra was recorded in DMSO-D_2O solvent mixtures.

^{1}H NMR (400 MHz, DMSO + D_2O) δ 8.88 (d, J = 8 Hz, 1 H), 8.60 (d, J = 8 Hz, 1 H), 8.21 (d, J = 8 Hz, 1 H), 7.92 (t, J = 8 Hz, 1 H), 7.71 – 7.67 (m, 1 H), 7.53 (d, J = 4 Hz, 1 H), 7.41 (t, J = 8 Hz, 1 H), 7.29 – 7.20 (m, 3 H), 7.14 (m, 2 H), 6.69 (d, J = 4 Hz, 1 H), 5.97 (d, J = 8 Hz, 1 H), 2.58 (m, 2 H), 1.00 (dd, J = 8, 4 Hz, 12 H).

Synthesis of 2-(2,6-diisopropylphenyl)-6-((7-fluoro-1H-indol-1-yl)amino)-1H-benzo[de]isoquinoline-1,3(2H)-dione (F-AINP):

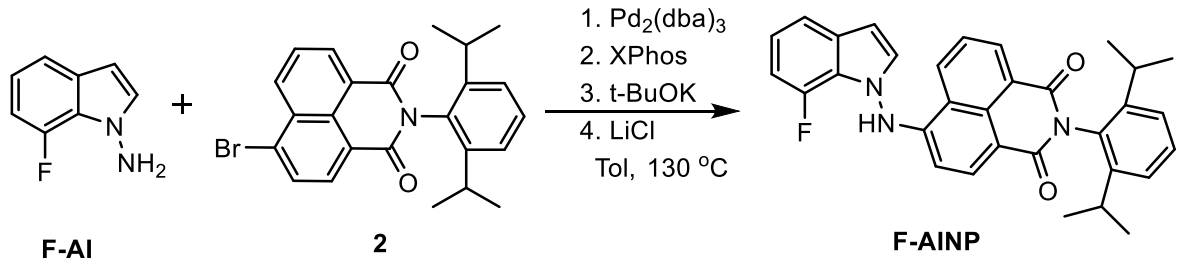

Scheme S5. Synthesis of 2-(2,6-diisopropylphenyl)-6-((7-fluoro-1H-indol-1-yl)amino)-1H-benzo[de]isoquinoline-1,3(2H)-dione (F-AINP).[S4]

Procedure: The mixture of compound **F-AI** (100 mg, 0.666 mmol) and **2** (242 mg, 0.555 mmol) were dissolved in toluene and degassed by freeze pump thaw method. In two neck round -bottomed flask, $Pd_2(dba)_3$ (2.5 mol%), XPhos (5 mol%), LiCl (47 mg, 1.11 mmol) and *t*-BuOK (93 mg, 0.832 mmol) were taken and simultaneously F-AI and 2 were added and stirred for 4-5 h at 110 ^{o}C. The reaction mixture was cooled and filtered through celite pad using ethyl acetate and the final compound was purified by column chromatography using ethyl acetate and hexane (10:90, v/v) as eluent.

^{1}H NMR (400 MHz, DMSO): δ (ppm) 11.26 (s, 1 H), 8.85 (d, J = 8.6 Hz, 1 H), 8.62 (d, J = 7.3 Hz, 1 H), 8.29 (s, 1 H), 7.97 – 7.92 (m, 1 H), 7.66 (d, J = 3.3 Hz, 1 H), 7.52 (d, J = 7.7 Hz, 1 H), 7.43 (t, J = 7.8 Hz, 1 H), 7.31 (d, J = 7.7 Hz, 2 H), 7.10 (m, J = 7.9, 4.5 Hz, 1 H), 6.97

(dd, *J* = 12.5, 7.6 Hz, 1 H), 6.78 (t, *J* = 2.8 Hz, 1 H), 6.09 (d, *J* = 8.4 Hz, 1 H), 2.69 – 2.61 (m, 2 H), 1.04 (t, *J* = 7.6 Hz, 12 H).

^{13}C NMR (400 MHz, DMSO) δ 163.95, 163.19, 150.82, 147.58, 134.29, 131.88, 131.41, 131.14, 130.86, 130.82, 129.49, 128.96, 128.73, 126.23, 123.64, 122.04, 121.04, 119.02, 117.44, 112.12, 105.35, 102.18, 28.57, 23.65.

ESI-TOF: $(M+H)^+$ of molecular formula $C_{32}H_{28}N_3O_2F$: Calculated 506.2244; found 506.2268.

2. ^{1}H and ^{13}C NMR spectra

^{1}H NMR of AI

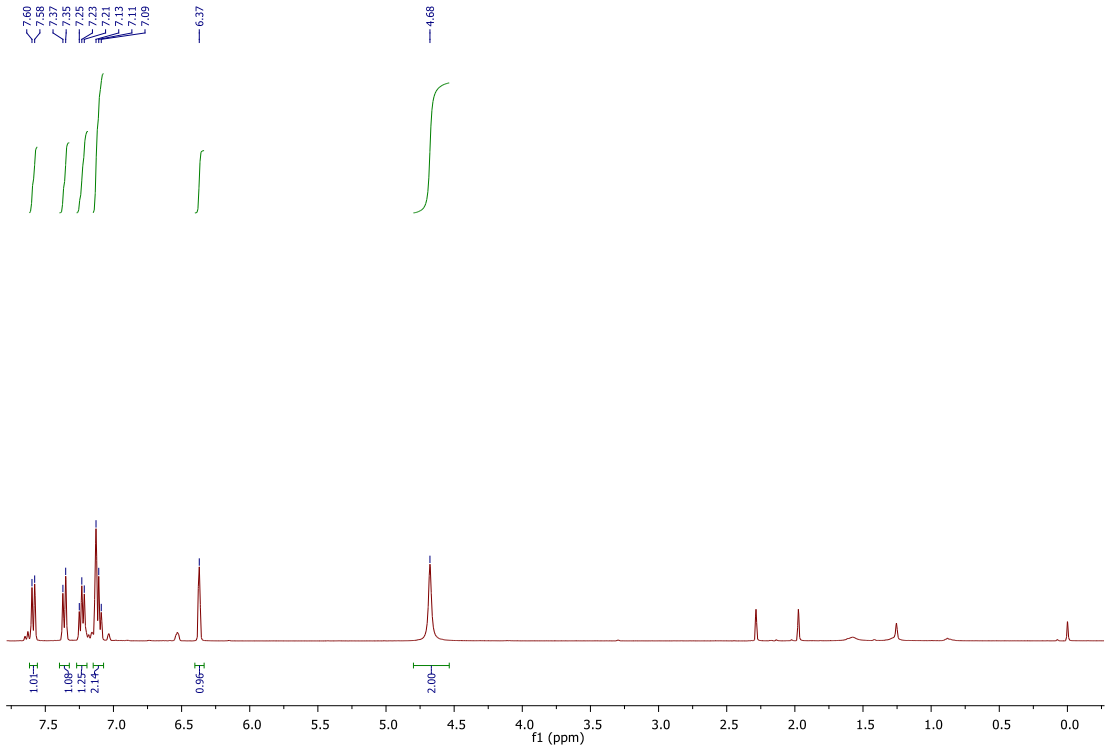

^{1}H NMR of NP

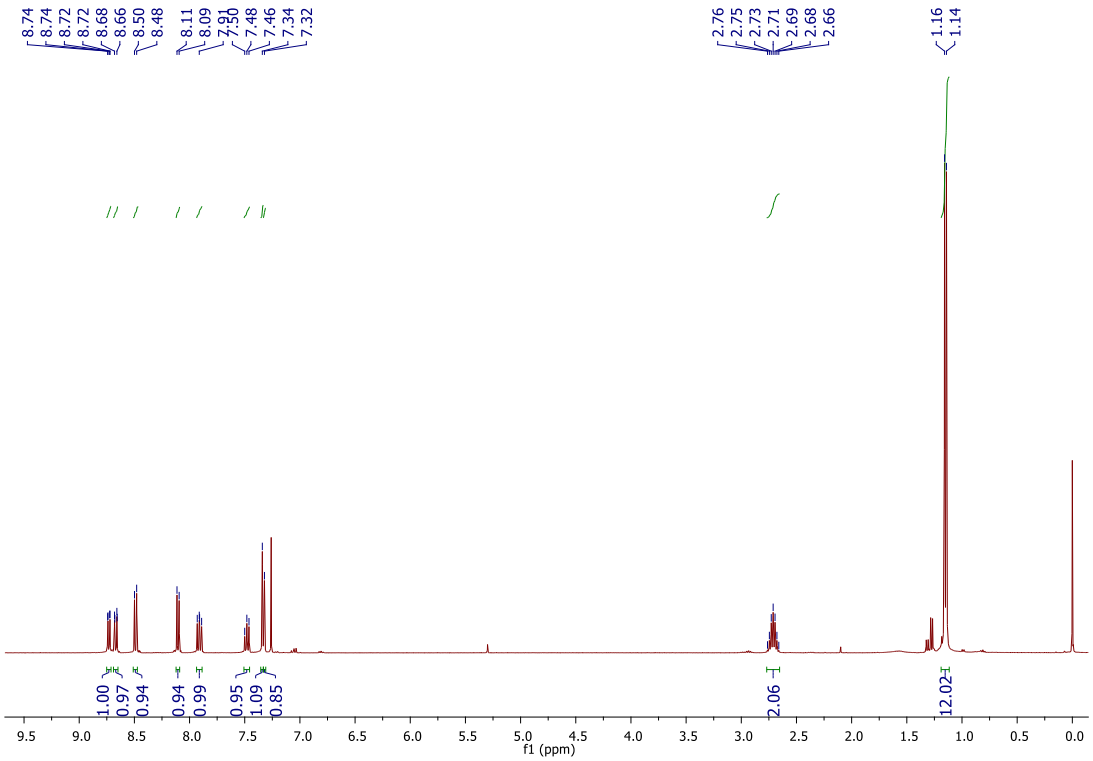

^{1}H NMR of AIN

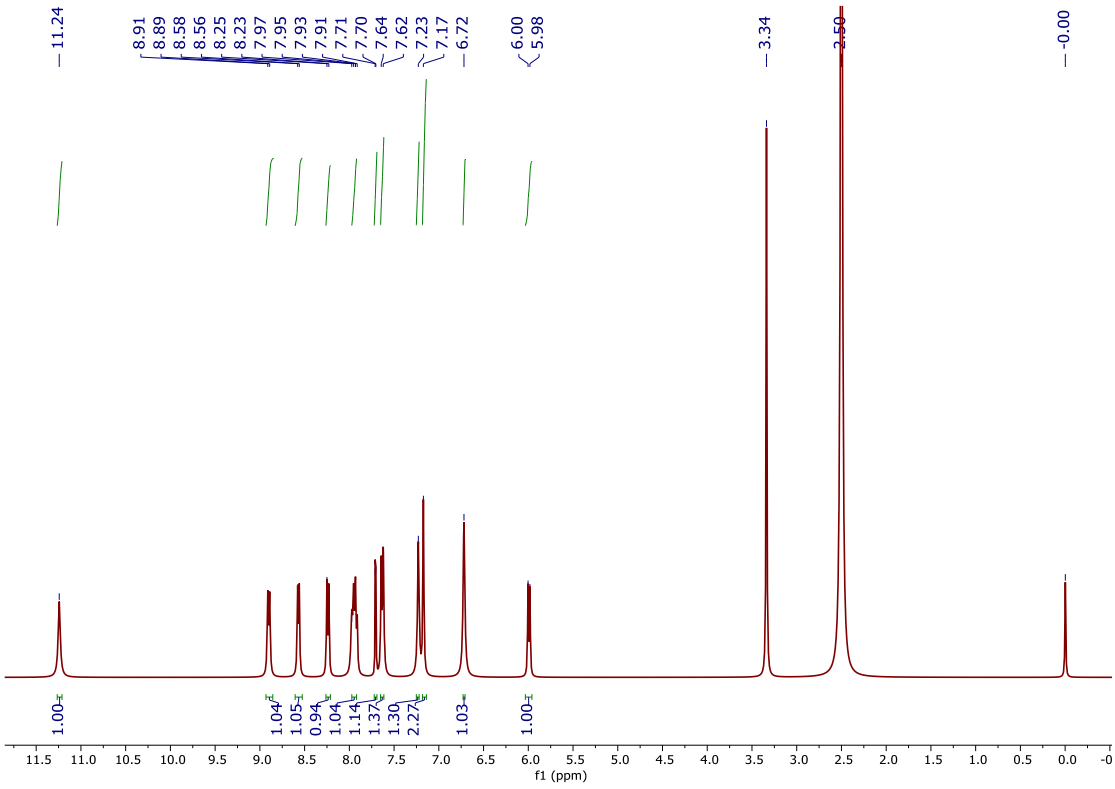

^{13}C NMR of AIN in DMSO

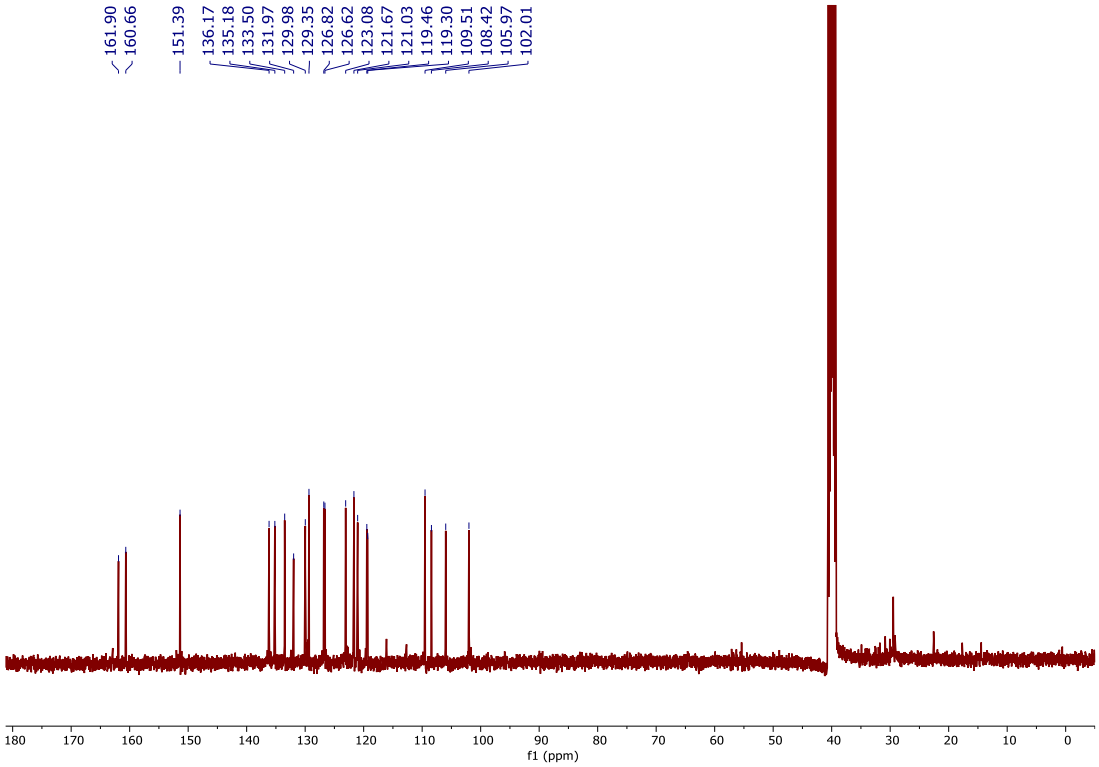

^{1}H NMR of AINP in DMSO

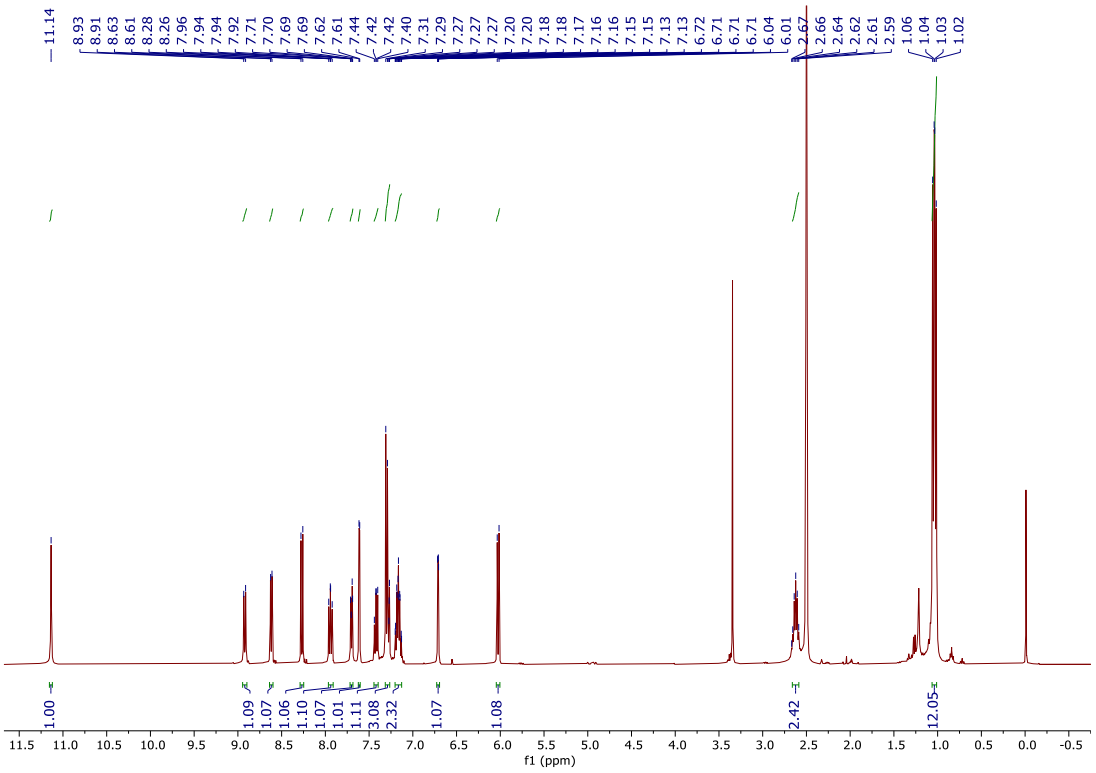

^{13}C NMR of AINP in DMSO

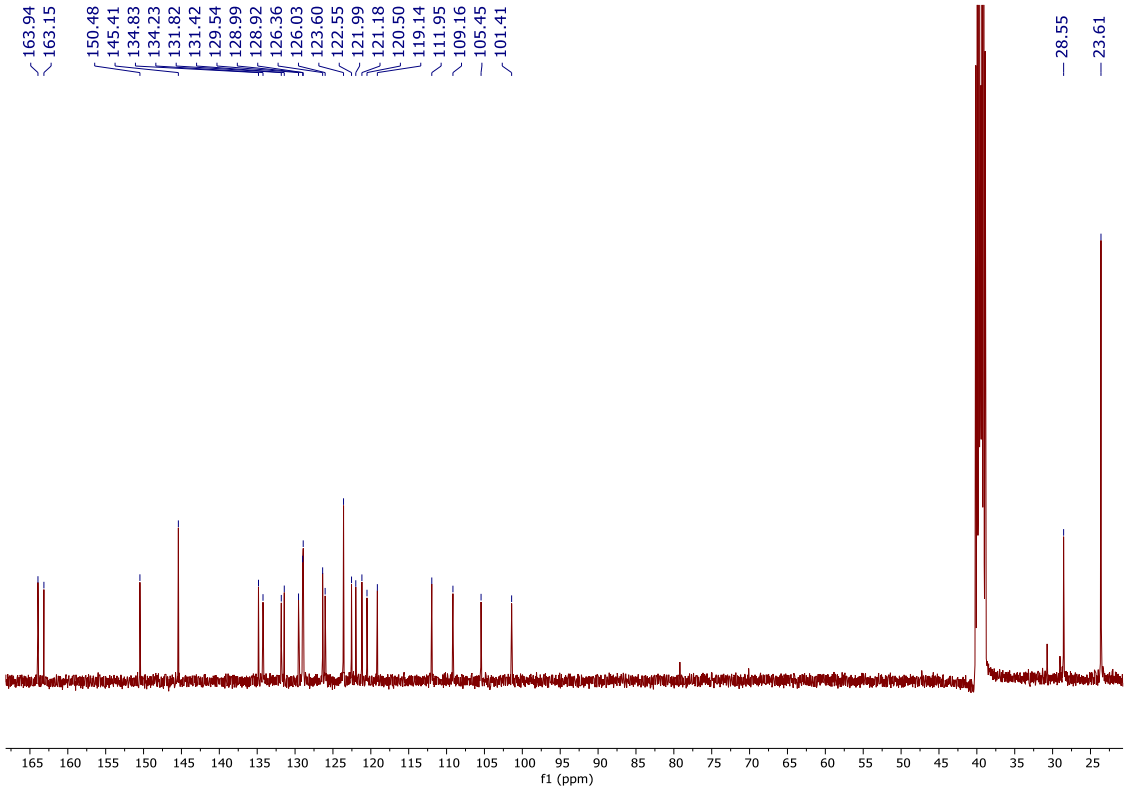

^{1}H NMR of AINP in DMSO & D_2O

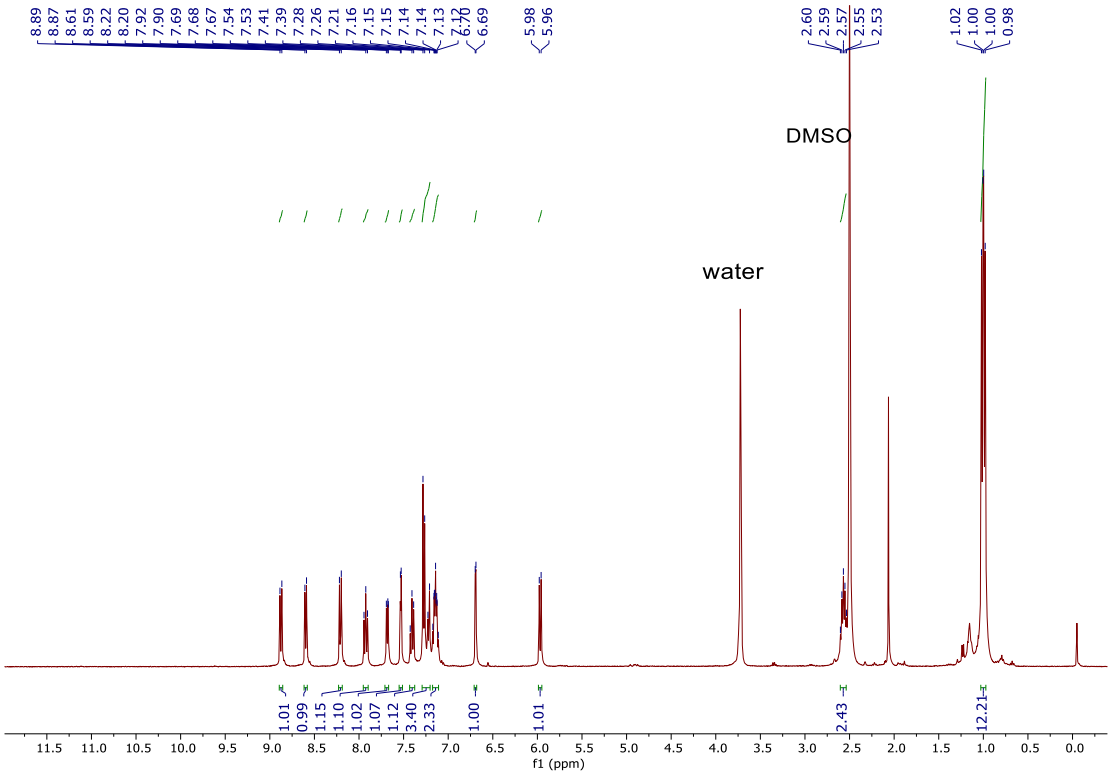

^{1}H NMR (400 MHz, DMSO) of F-AINP:

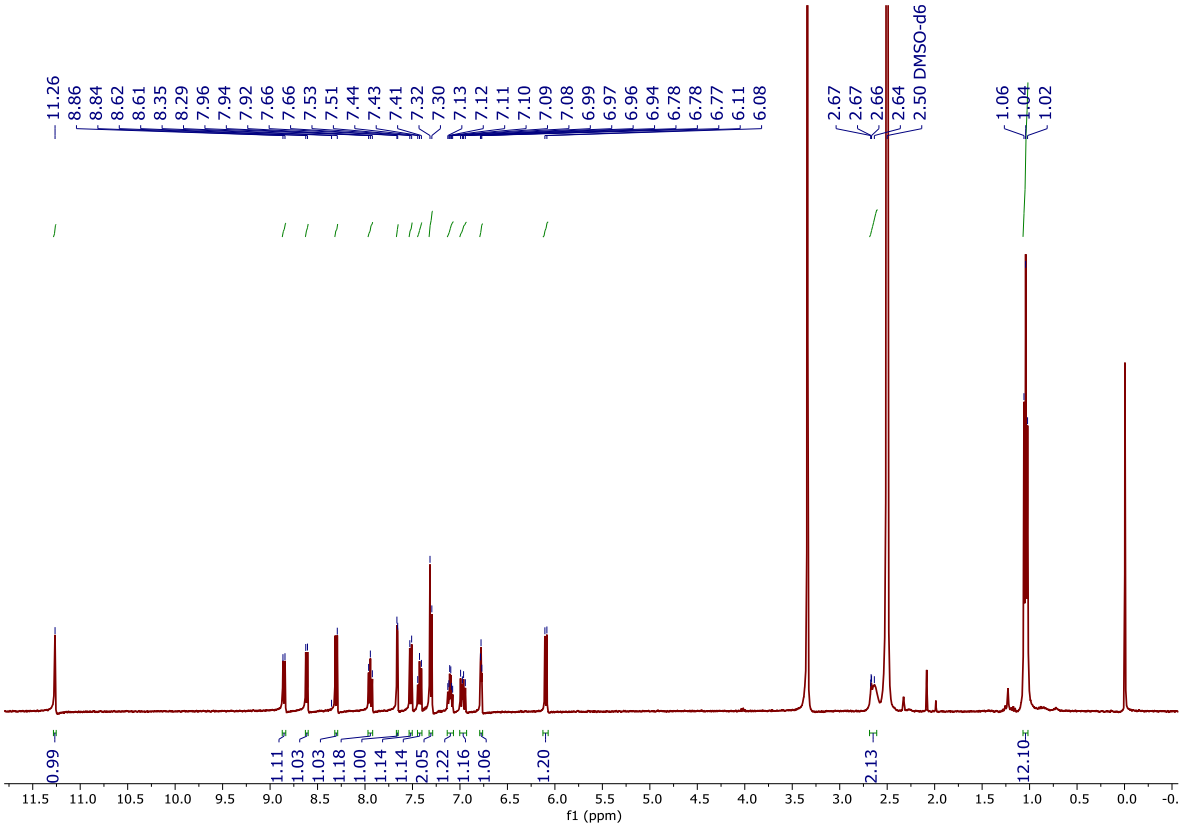

^{13}C NMR (400 MHz, DMSO) of F-AINP:

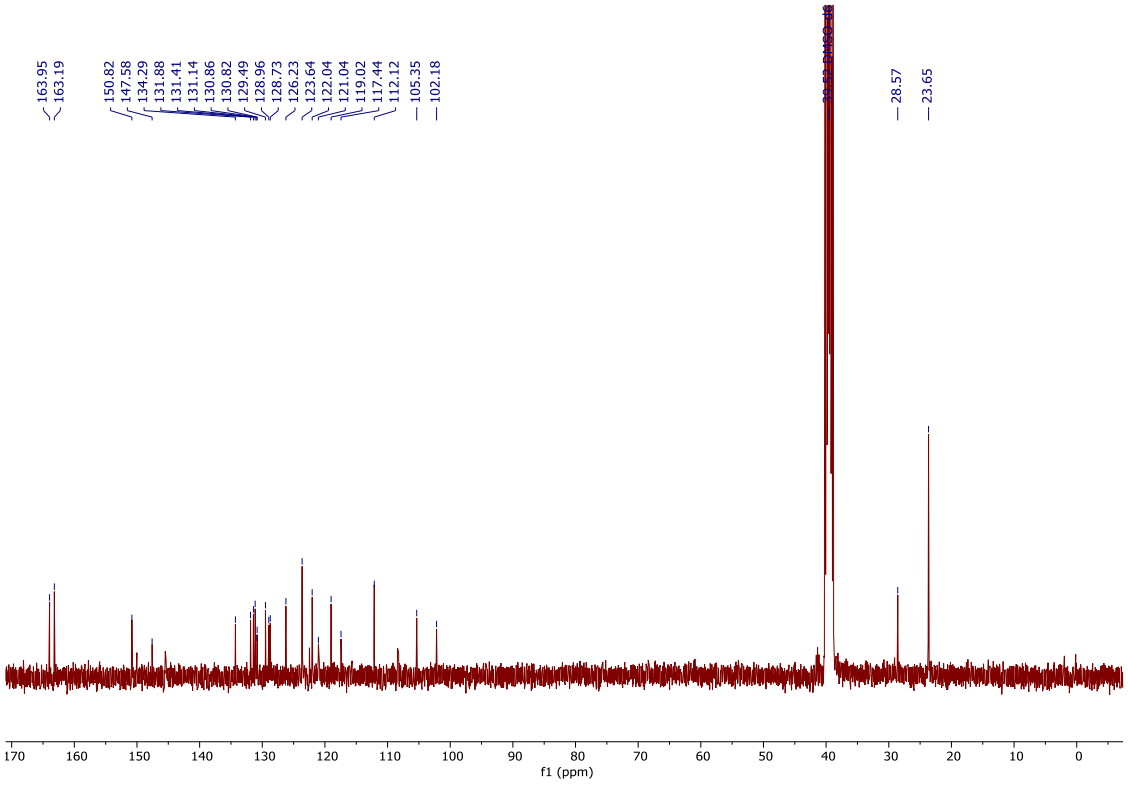

Concentration dependent ^{1}H-NMR of AINP in DMSO:

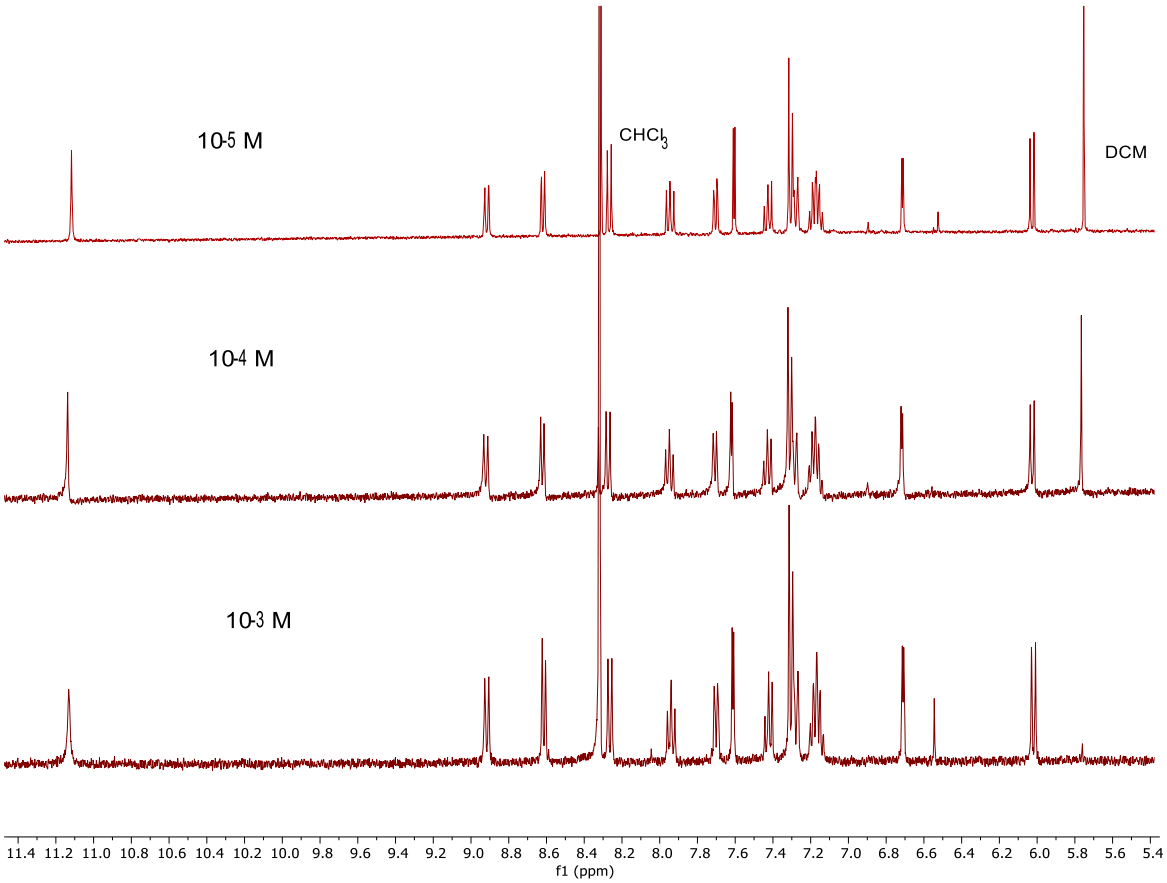

3. UV/Vis Absorption and Emission Spectra

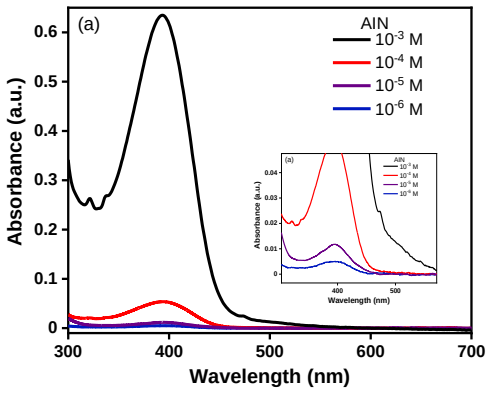

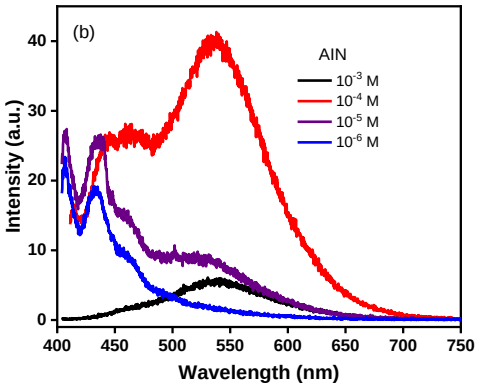

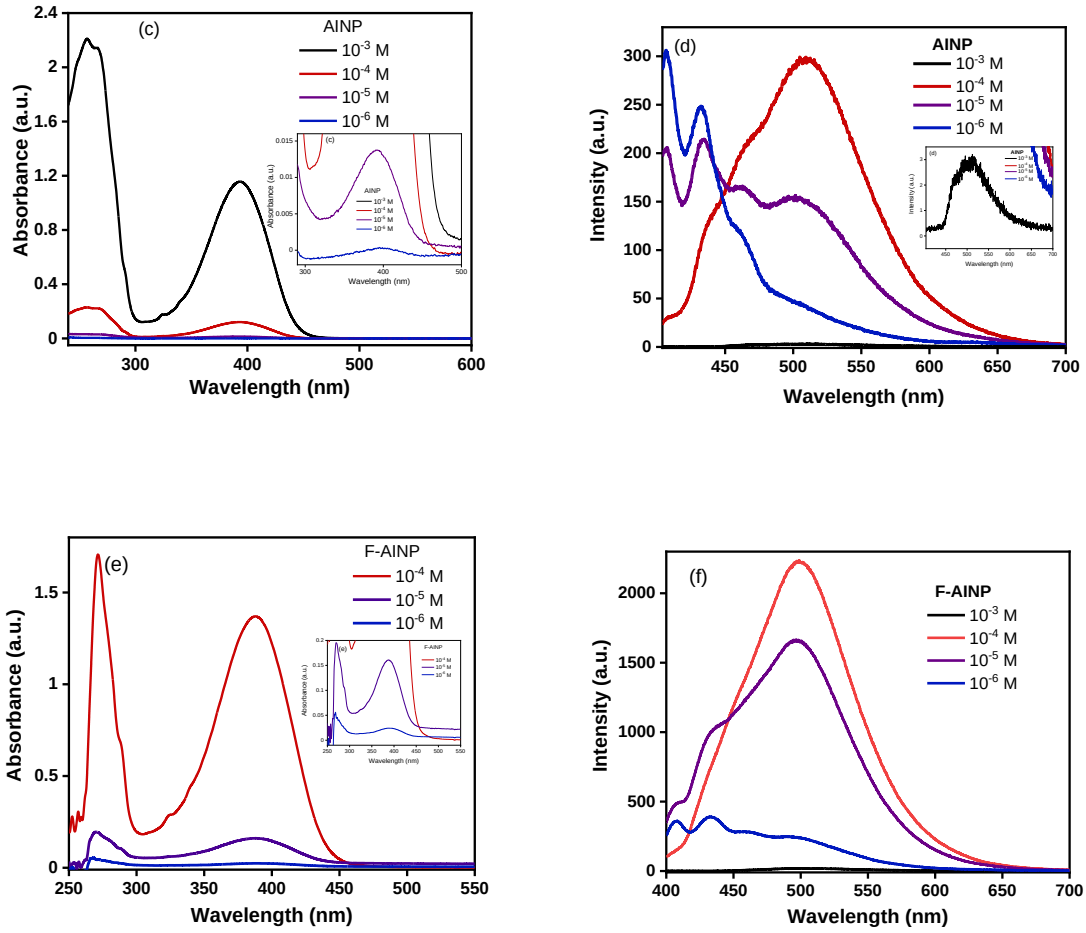

Figure S1. Concentration dependent UV/Vis absorption of (a) **AIN**, (c) **AINP** and (e) **F-AINP** and emission (b) **AIN** (λ_{ex} = 394 nm), (d) **AINP** (λ_{ex} = 393 nm) and (f) **F-AINP** (λ_{ex} = 388 nm).

4. Fluorescence Quantum Yield

Fluorescence quantum yield was measured by using relative method using 4',6-diamidino-2-phenylindole (DAPI, Φ_R = 0.58) in DMSO as reference dyes and using the following equation:[S5]

$$\mathbf{\Phi = \Phi_R\,(I/I_R)\,(A_R/A)\,(\lambda_{exR}/\lambda_{ex})\,(n^2/n^2{}_R)}$$

where Φ_R is the quantum yield of reference dye DAPI in DMSO, I and I_R are integrated fluorescence intensities of compounds and reference dye respectively, A and A_R are the absorbance of the compounds and reference dye respectively, and n and n_R are the refractive

indices of solvent(s) used for compounds and reference respectively. The compounds **AIN**, **AINP** and **F-AINP** were dissolved in $CHCl_3$ in three different concentrations ($c \sim 10^{-5}$-10^{-6} M) such that their absorbance was less than or equal to 0.1 and their absorption and fluorescence spectra were recorded (at excitation wavelengths of 388 nm, 394 nm, 394 nm for **AIN**, **AINP** and **F-AINP** respectively). Absorbance and fluorescence spectra were recorded for three different concentrations of DAPI (excitation wavelength of ~ 360 nm) in DMSO ($c \sim 10^{-5}$-10^{-6} M). Fluorescence quantum yields were then calculated using the above equation for each compound.

Table S1: Relative quantum yields of **AIN**, **AINP** and **F-AINP** using relative method and DAPI as a reference dye.

Compound	**Absorbance**			**Integrated Fluorescence Intensity**			**Quantum Yield** $\Phi=\Phi_R(I/I_R)(A_R/A)(\lambda_{exR}/\lambda_{ex})(n^2/n^2_R)$	
	1	**2**	**3**	**1**	**2**	**3**	Φ_i	Φ_{avg}
AIN	0.0712	0.089	0.0104	79.56	71.45	61.03	0.040 0.033 0.023	0.032
AINP	0.0821	0.0906	0.0985	130.31	138.13	140.51	0.055 0.061 0.053	0.056
F-AINP	0.0557	0.0721	0.086	532.14	661.87	785.07	0.331 0.367 0.341	0.346

DAPI (DMSO)	0.0448	0.0707	0.0828	629.732	867.144	1086.253	0.58 (reported value)

5. Temperature Effect on ^{1}H-NMR of F-AINP:

To confirm the H-bonding in **F-AINP**, temperature dependent ^{1}H-NMR was recorded in $CHCl_3$ over the range of 233-313 K as shown in figure S2. Due to strengthening of H-bonding at lower temperature, NH- peak was observed to be deshielded with lowering of temperature[S6].

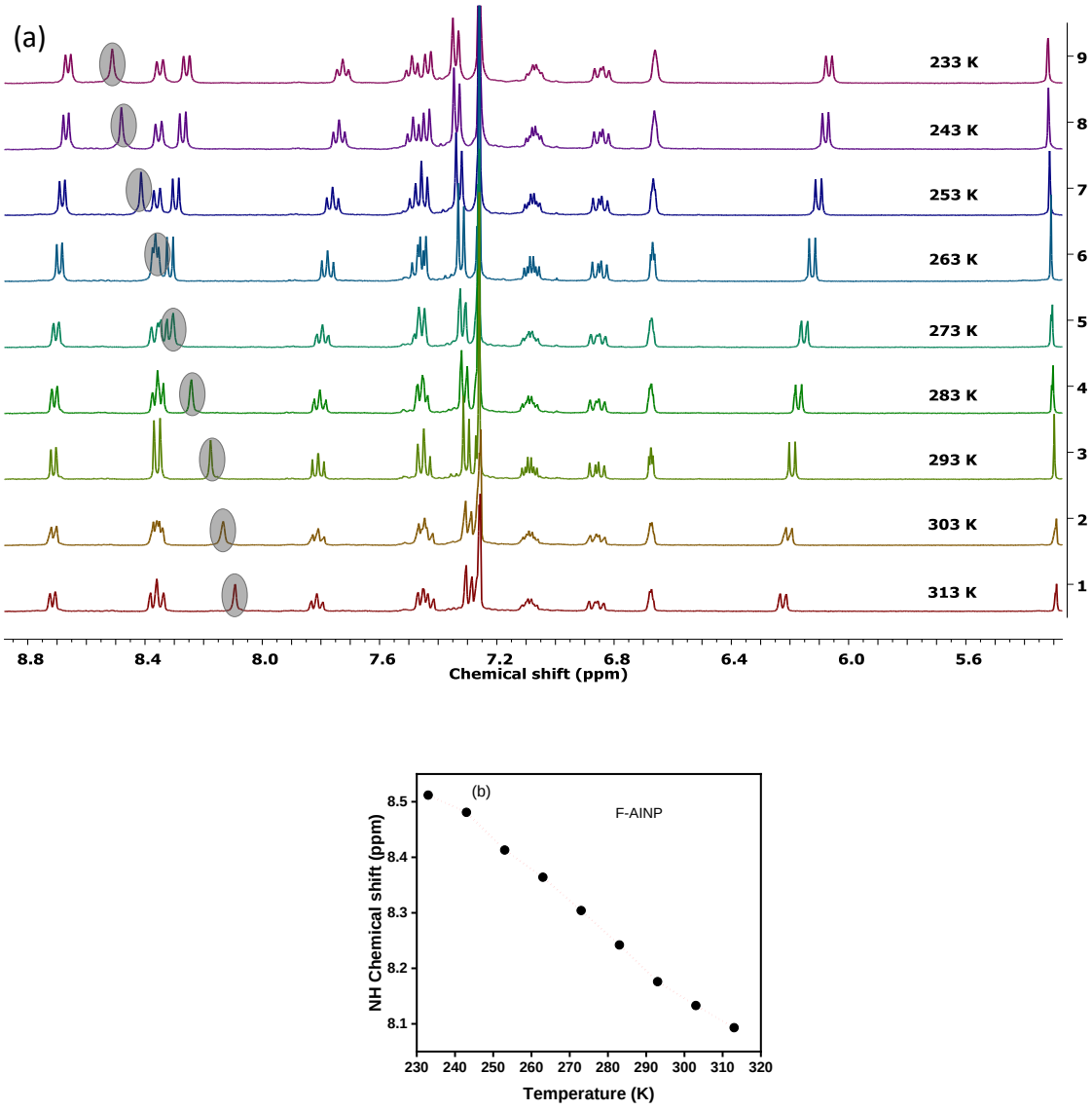

Figure S2. (a) Effect of temperature on ^{1}H-NMR and (b) plot of change of chemical shift of NH- peak vs temperature of **F-AINP**.

6. Solvatochromism:

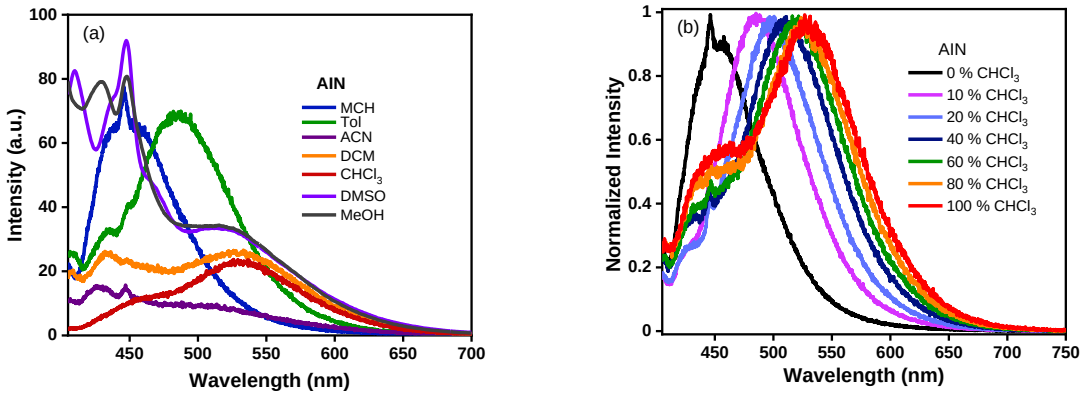

Figure S3. Emission of **AIN** (λ_{ex} = 394 nm), (a) in solvent of different polarity and (b) in different percentage of $CHCl_3$/MCH excited at (c ~10^{-5} M) respectively (inside the box, 0 %, 10 % to 100 % indicate the percentage of $CHCl_3$ in solutions).

7. Cyclic Voltammetry:

Cyclic voltammetry (CV) measurements were performed for **AIN**, **AINP** and **F-AINP** in dry DCM with 0.1 M tetrabutylammonium hexafluorophosphate as supporting electrolyte and Ag/AgCl as reference electrode to determine the HOMO and LUMO energy levels. Based on the first oxidation potential onset (E_{onset}^{ox}) and first reduction potential (E_{onset}^{red}), the HOMO and LUMO were calculated[S7] as,

HOMO = $-(E_{onset}^{ox} + 4.76)$ eV, and

LUMO = $-(E_{onset}^{red} + 4.76)$ eV

The cyclic voltammograms of all compounds are presented in figure S4 and the E_{onset}^{ox} and E_{onset}^{red} values as well as the calculated HOMO and LUMO values have been tabulated in table 1. Accordingly, the calculated HOMO energies for **AIN**, **AINP** and **F-AINP** are -5.85 eV, -5.89 eV and -5.93 eV respectively and LUMO energies are -3.93 eV, -3.86 eV and -3.90 eV respectively. In case of **F-AINP**, the HOMO energy level decreased due to fluorine atom attached at indole part.

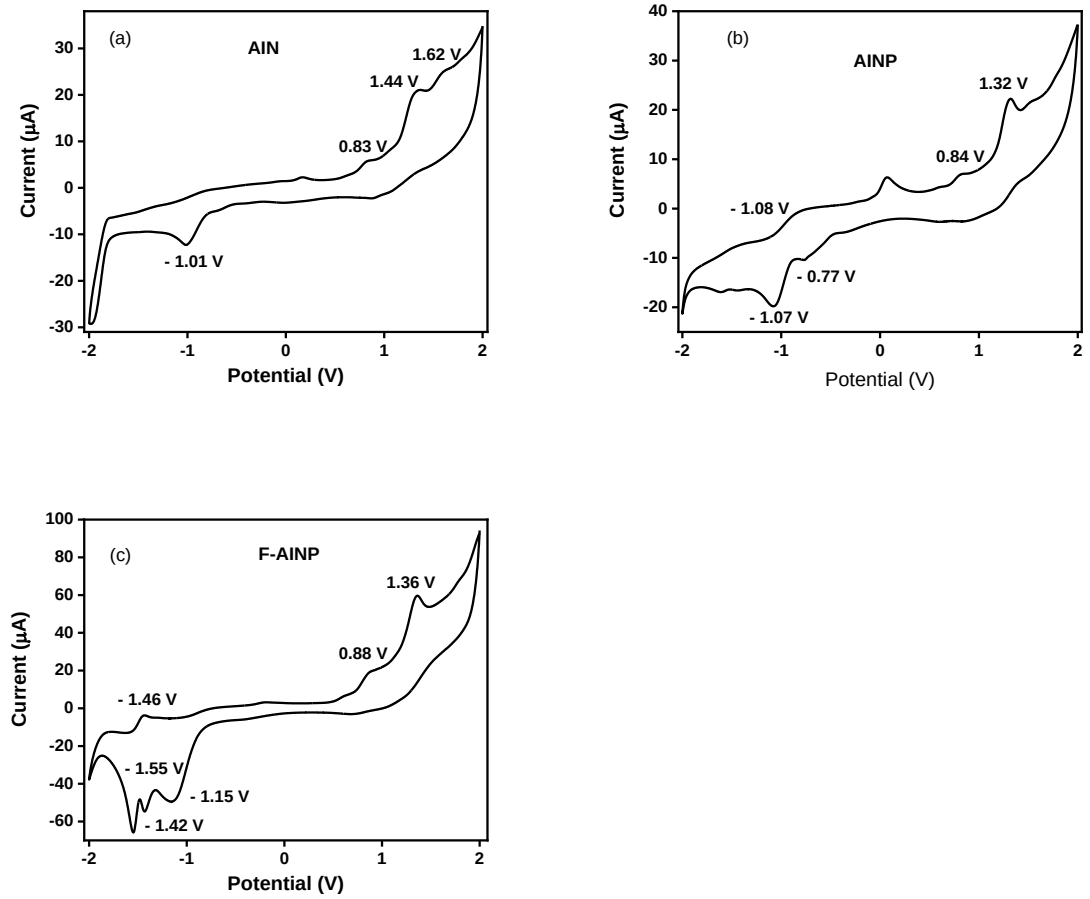

Figure S4. Cyclic voltammogram of (a) **AIN**, (b) **AINP**, (c) **F-AINP** in dry dichloromethane with 0.1 M tetrabutylammonium hexafluorophosphate (TBAHPF) and potentials measured vs Ag/AgCl reference electrode.

8. DFT Calculations:

Density functional theory (DFT) calculations were performed for all molecules in the ground state using the Gaussian 09 package[S1] at the B3LYP/6-31G(d,p) level to calculate the HOMO and LUMO energy levels as well as torsion angles in geometry optimized structures. The DFT calculated energy levels and dihedral angle are presented in the figure S5 and table S2. In case of **AIN**, the calculated HOMO and LUMO energy levels were – 6.00 eV and – 2.59 eV (table S2) respectively. HOMO was completely localized on aminoindole part while the LUMO and LUMO +1 were localized on naphthalimide part as shown in figure S5. Hence, charge transfer can be observed from HOMO to LUMO as well as HOMO to LUMO +1. Similarly, in case of **AINP,** the calculated HOMO and LUMO energy levels were – 5.87 eV and – 2.30 eV respectively and HOMO was localized on aminoindole part as well as small portion on

naphthalimide part while LUMO and LUMO +1 were completely localized on naphthalimide and hence, CT can be observed from HOMO to LUMO as well as HOMO to LUMO +1. While in case of **F-AINP**, the calculated HOMO and LUMO energy levels were – 5.93 eV and – 2.25 eV respectively and HOMO was localized on aminoindole as well as on naphthalimide and LUMO and LUMO +1 were localized on naphthalimide part. Hence, CT can be observed from HOMO to LUMO as well as HOMO to LUMO +1.

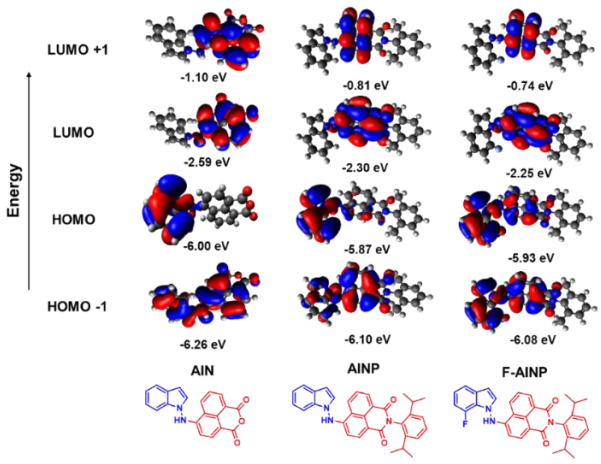

Figure S5. FMO energy levels of compounds **AIN**, **AINP** and **F-AINP** calculated using B3LYP/6-31G(d,p).

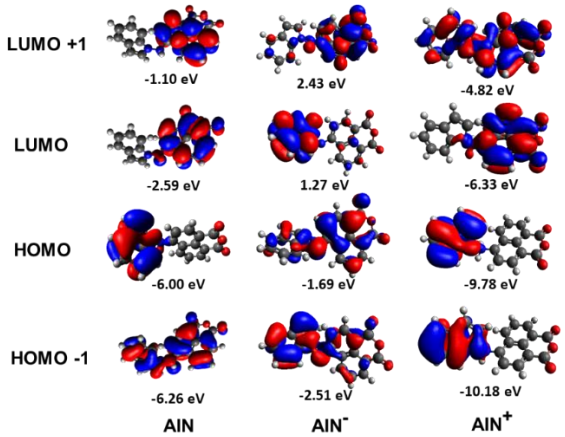

Figure S6. DFT calculated (B3LYP/6-31G(d,p)) geometry optimized structures of **AIN**, **AIN**$^{-}$ and **AIN**$^{+}$ with energy levels.

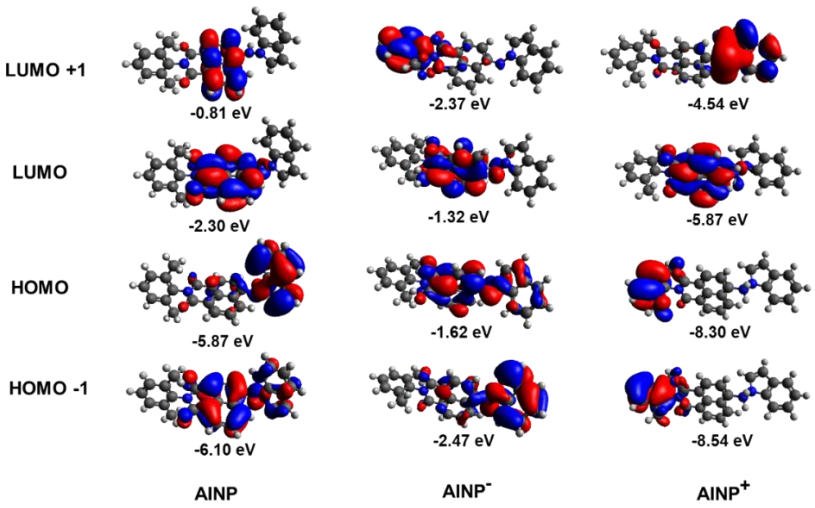

Figure S7. DFT calculated (B3LYP/6-31G(d,p)) geometry optimized structures of **AINP**, **AINP**$^{-}$ and **AINP**$^{+}$ with energy levels.

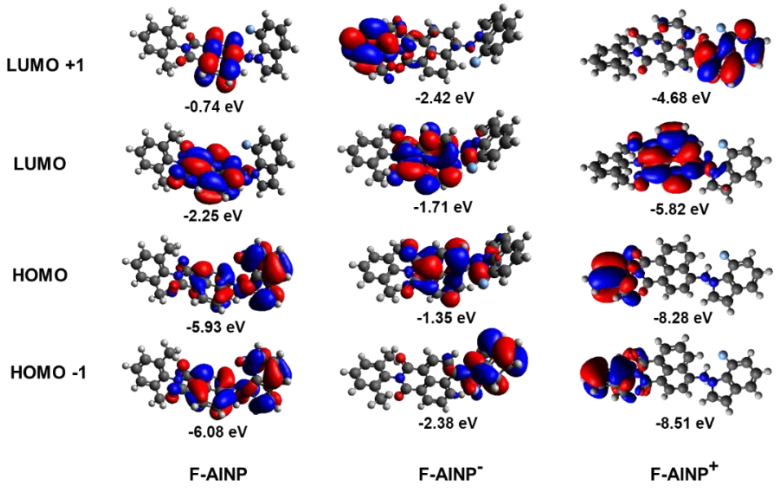

Figure S8. DFT calculated (B3LYP/6-31G(d,p)) geometry optimized structures of **F-AINP**, **F-AINP**$^{-}$ and **F-AINP**$^{+}$ with energy levels.

Table S2: Dihedral angles (in degrees), HOMO and LUMO (eV) energy levels and bond length calculated by B3LYP/6-31G (d,p) method for dyads and triads.

Compounds	HOMO (eV)	LUMO (eV)	ΔE (eV)	Dihedral angle (°) (C_1-N_2-N_3-C_4)	Bond length (Å)		
					C_1-N_2	N_2-N_3	N_3-C_4
AIN	- 6.00	- 2.59	3.41	106.2	1.39	1.38	1.39
AIN$^-$	- 1.69	1.27	2.96	71.7	1.38	1.40	1.32
AIN$^+$	- 9.78	- 6.33	3.45	60.2	1.42	1.46	1.48
AINP	- 5.87	- 2.30	3.57	126.9	1.39	1.38	1.41
AINP$^-$	- 1.62	1.32	2.94	- 71.7	1.38	1.40	1.33
AINP$^+$	- 8.30	- 5.87	2.43	58.4	1.42	1.46	1.48
F-AINP	- 5.93	- 2.25	3.68	122.5	1.39	1.39	1.41
F-AINP$^-$	- 1.71	1.35	3.06	- 98.7	1.37	1.41	1.33
F-AINP$^+$	- 8.28	- 5.82	2.46	67.3	1.42	1.46	1.47

9. Temperature-dependent Emission:

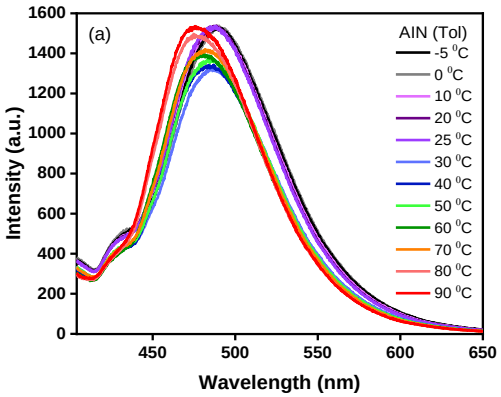

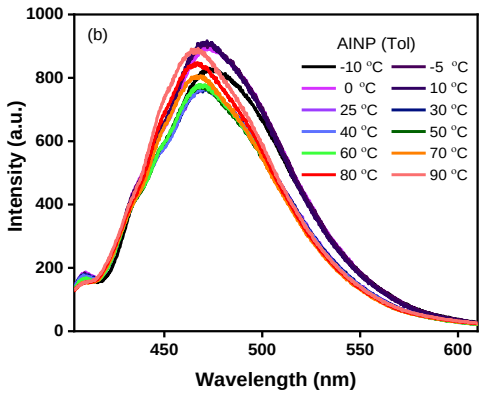

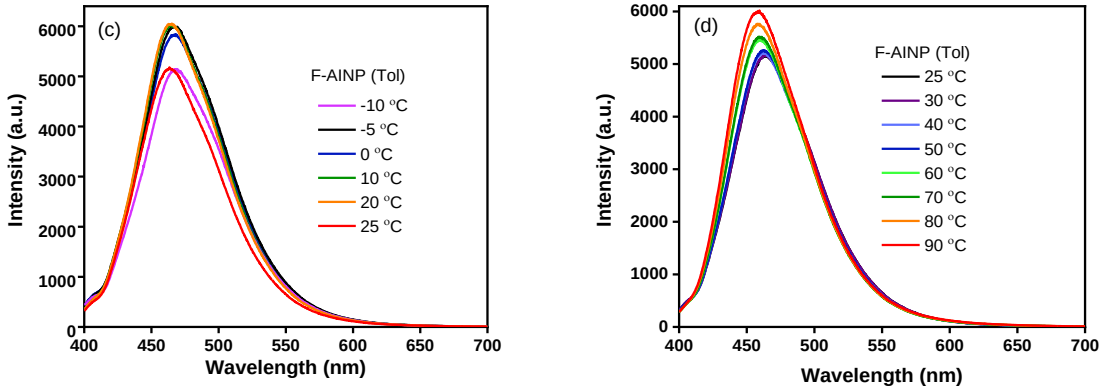

Figure S9. Temperature-dependent emission spectra of (a) **AIN** (λ_{ex} = 394 nm), (b) **AINP** (λ_{ex} = 393 nm) and (c), (d) **F-AINP** (λ_{ex} = 388 nm) in toluene in 10^{-5} M concentration.

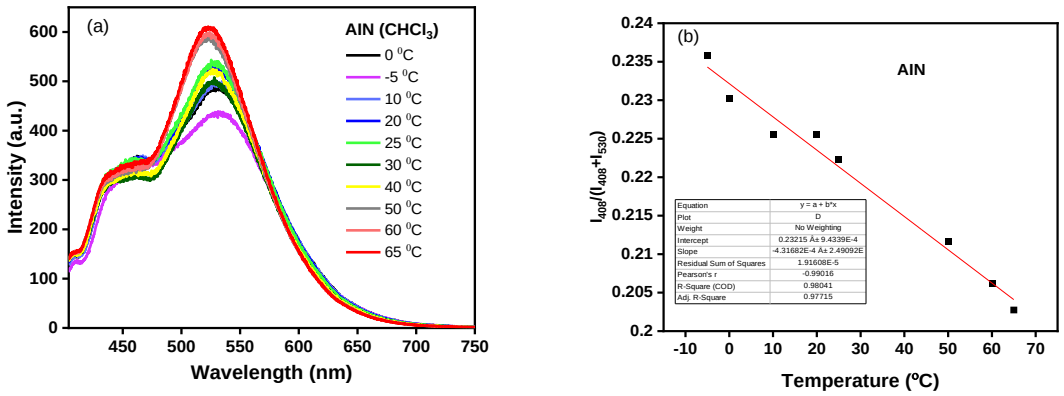

Figure S10. (a) Temperature-dependent emission spectra and (b) emission intensity ratio with best fit equation of **AIN** in $CHCl_3$ at different temperature (c ~ 10^{-5} M).

Table S3. Fitted parameters for temperature dependent fluorescence intensities and sensitivity for **AIN**, **AINP** and **F-AINP** in $CHCl_3$.

Compounds	**R^2**	**Equation** **$Y = I_1/(I_1+I_2)$, x = T (˚C)**	**Sensitivity** **% ˚C^{-1}**
AIN	0.98	$Y = -4.31\ e^{-4} + 0.23$	- 0.04
AINP	0.87	$Y = -8.71\ e^{-4} + 0.17$	- 0.08
F-AINP	0.86	$Y = -1.02\ e^{-3} + 0.20$	- 0.1

10. Viscosity Dependent Emission:

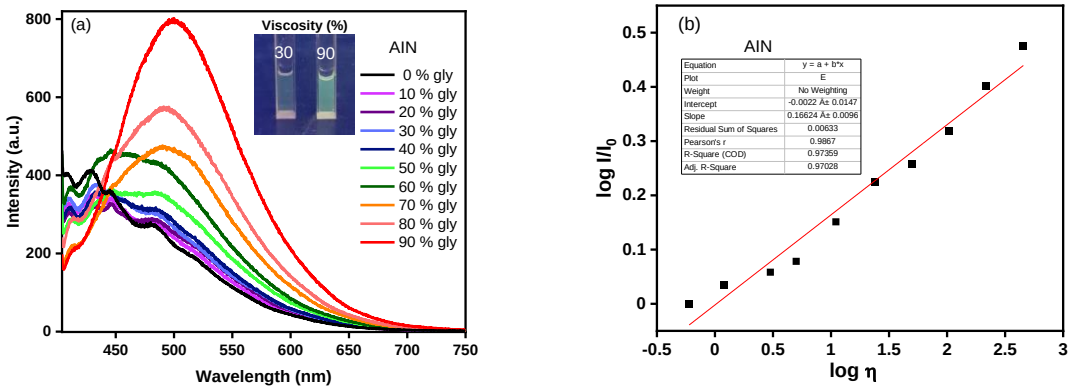

Figure S11. (a) Viscosity dependent emission spectra in gly/MeOH mixtures and (b) emission intensity ratio of **AIN** (λ_{ex} = 394 nm) at different viscosity of solution with best fit equations.

11. Temperature-dependent Emission Spectra at gly/methanol 70/30 (v/v):

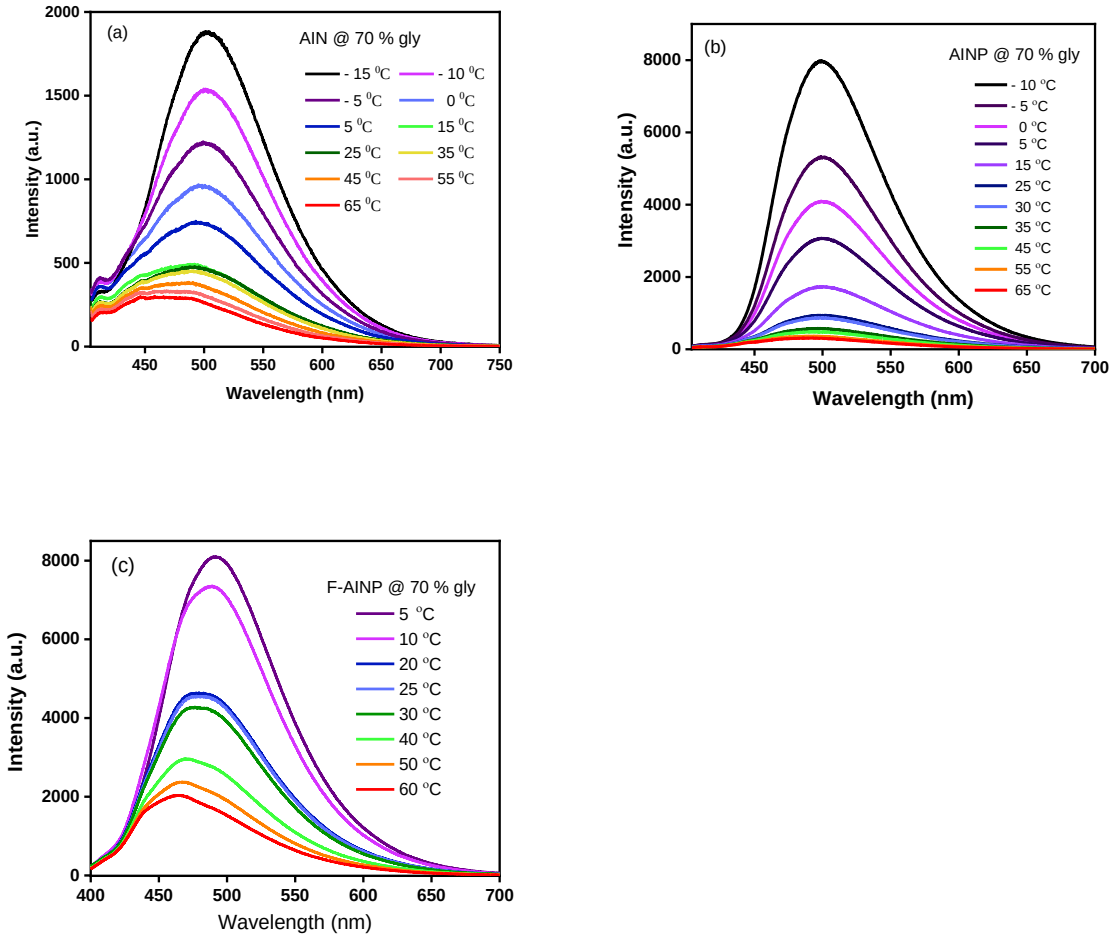

Figure S12. Temperature-dependent emission spectra of (a) **AIN**, (b) **AINP** and (c) **F-AINP** in glycerol/methanol 70/30 v/v (104 cP) solution.

12. Fluorescence Lifetime:

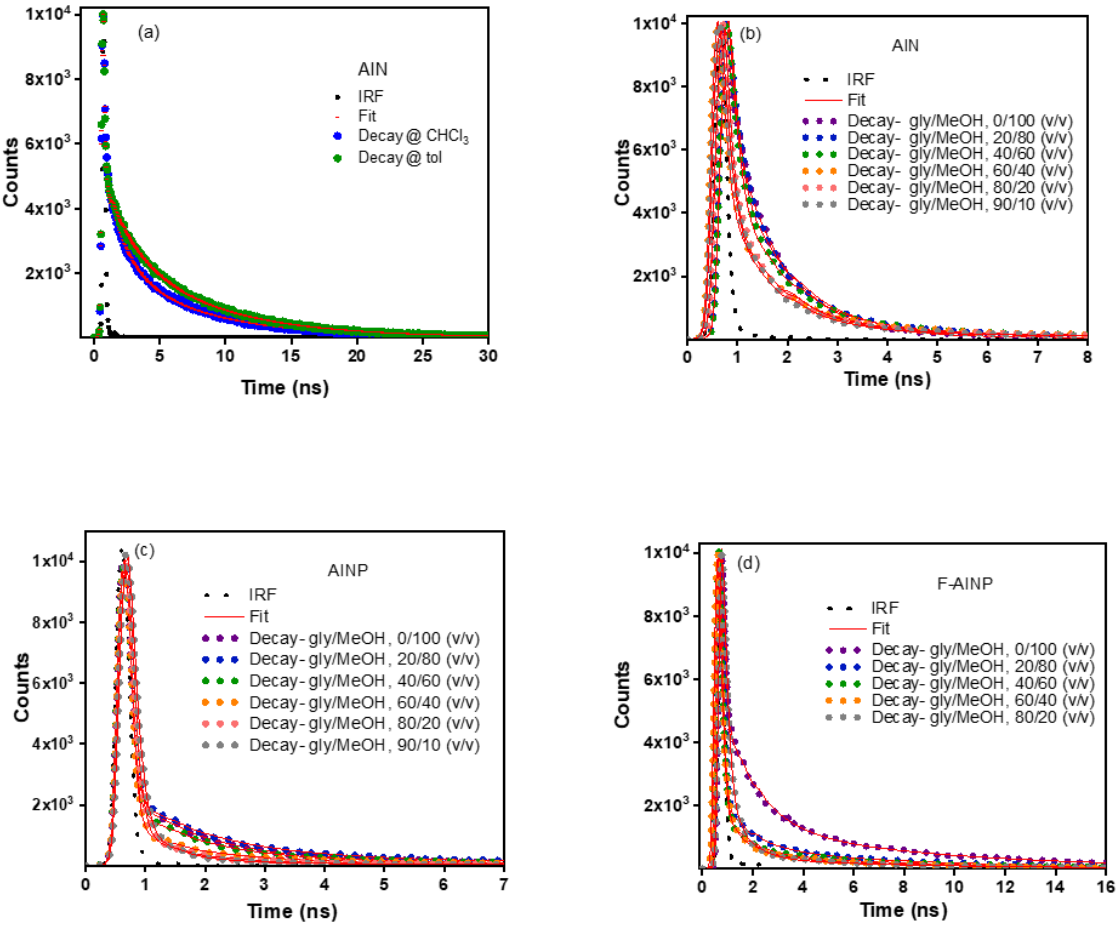

Figure S13. Fluorescence lifetime decay collected using a single photon counting technique (a) in $CHCl_3$ and Tol of **AIN** and in solvent of different viscosities for (b) **AIN** (c) **AINP** and (d) **F-AINP**.

Table S4. Fluorescence lifetime analyses of **AIN**, **AINP** and **F-AINP** at different emission wavelength.

Compound (λ_{ex} = 375 nm)	**Solvent**	λ_{em} **(nm)**	$\tau_1(\alpha_1)$ **(ns)**	$\tau_2(\alpha_2)$ **(ns)**	$\tau_3(\alpha_3)$ **(ns)**	τ_{avg} **(ns)**	χ^2
AIN	$CHCl_3$	530	1.47 (0.03)	6.73 (0.02)	0.038 (0.96)	0.20	1.09
	Tol	485	2.37 (0.03)	7.39 (0.04)	0.053 (0.93)	0.41	1.03
	$^*CHCl_3$	510	-	-	-	-	-

AINP	Tol	470	1.16 (0)	6.46 (0)	0.02 (1.0)	0.04	0.86
F-AINP	$CHCl_3$	500	1.27 (0.01)	6.73 (0.01)	0.035 (0.98)	0.11	1.01
	*Tol	464	-	-	-	-	-

*Lifetime not detected.

Table S5: Fluorescence decay parameters of **AIN**, **AINP** and **F-AINP** at variable viscosity[S8], the decay times (τ_1, τ_2 and τ_3) and the respective fractional contributions (α_1, α_2 and α_3), the amplitude average decay time (τ_{avg}) and the quality of fitting (χ^2).

Compound (λ_{ex} = 375nm)	**Viscosity (in cP) (solvent mixture)**	**$\tau_1(\alpha_1)$ (ns)**	**$\tau_2(\alpha_2)$ (ns)**	**$\tau_3(\alpha_3)$ (ns)**	**Average lifetime τ_{avg} (ns)**	**χ^2**
AIN	454 (90/10 v/v gly/MeOH)	0.98 (0.17)	0.15 (0.82)	8.45 (0.01)	0.37	1.17
	218 (80/20 v/v gly/MeOH)	0.98 (0.12)	8.42 (0.01)	0.09 (0.87)	0.26	1.28
	50 (60/40 v/v gly/MeOH)	1.02 (0.11)	8.77 (0.01)	0.08 (0.88)	0.25	1.28
	11 (40/60 v/v gly/MeOH)	0.06 (0.19)	8.76 (0.01)	0.01 (0.80)	0.39	1.31
	3 (20/80 v/v gly/MeOH)	1.01 (0.23)	7.18 (0.01)	0.01 (0.76)	0.4	1.30
	0.6 (0/100 v/v gly/MeOH)	0.14 (0.58)	0.9 (0.41)	5.11 (0.01)	0.49	1.29
AINP	454 (90/10 v/v gly/MeOH)	1.33 (0.03)	7.76 (0)	0.08 (0.96)	0.15	1.22
	218 (80/20 v/v gly/MeOH)	1.12 (0.01)	7.82 (0)	0.02 (0.99)	0.04	1.15
	50 (60/40 v/v gly/MeOH)	1.35 (0)	8.71 (0)	0.002 (1)	0.002	1.29
	11 (40/60 v/v gly/MeOH)	1.4 (0)	0.003 (1)	8.97 (0)	0.003	1.24
	3 (20/80 v/v gly/MeOH)	0.003 (1)	1.26 (0)	7.66 (0)	0.003	1.23
	0.6 (0/100 v/v gly/MeOH)	0.002 (1)	1.16 (0)	5.1 (0)	0.002	1.21
F-AINP	454 (90/10 v/v gly/MeOH)	0.78 (0.09)	6.63 (0.01)	0.16 (0.89)	0.3	1.22
	218 (80/20 v/v gly/MeOH)	0.92 (0.02)	6.9 (0.01)	0.05 (0.97)	0.12	1.21
	50 (60/40 v/v gly/MeOH)	1.16 (0.01)	7.14 (0)	0.03 (0.99)	0.06	1.18
	11 (40/60 v/v gly/MeOH)	1.44 (0)	7.38 (0)	0.003 (1)	0.003	1.20
	3 (20/80 v/v gly/MeOH)	1.38 (0)	7.48 (0)	0.003 (1)	0.003	1.15

	0.6 (0/100 v/v gly/MeOH)	1.28 (0)	7.51 (0)	0.006 (1)	0.006	1.22

13. UV/Vis Absorption Spectra in Water and THF Mixture:

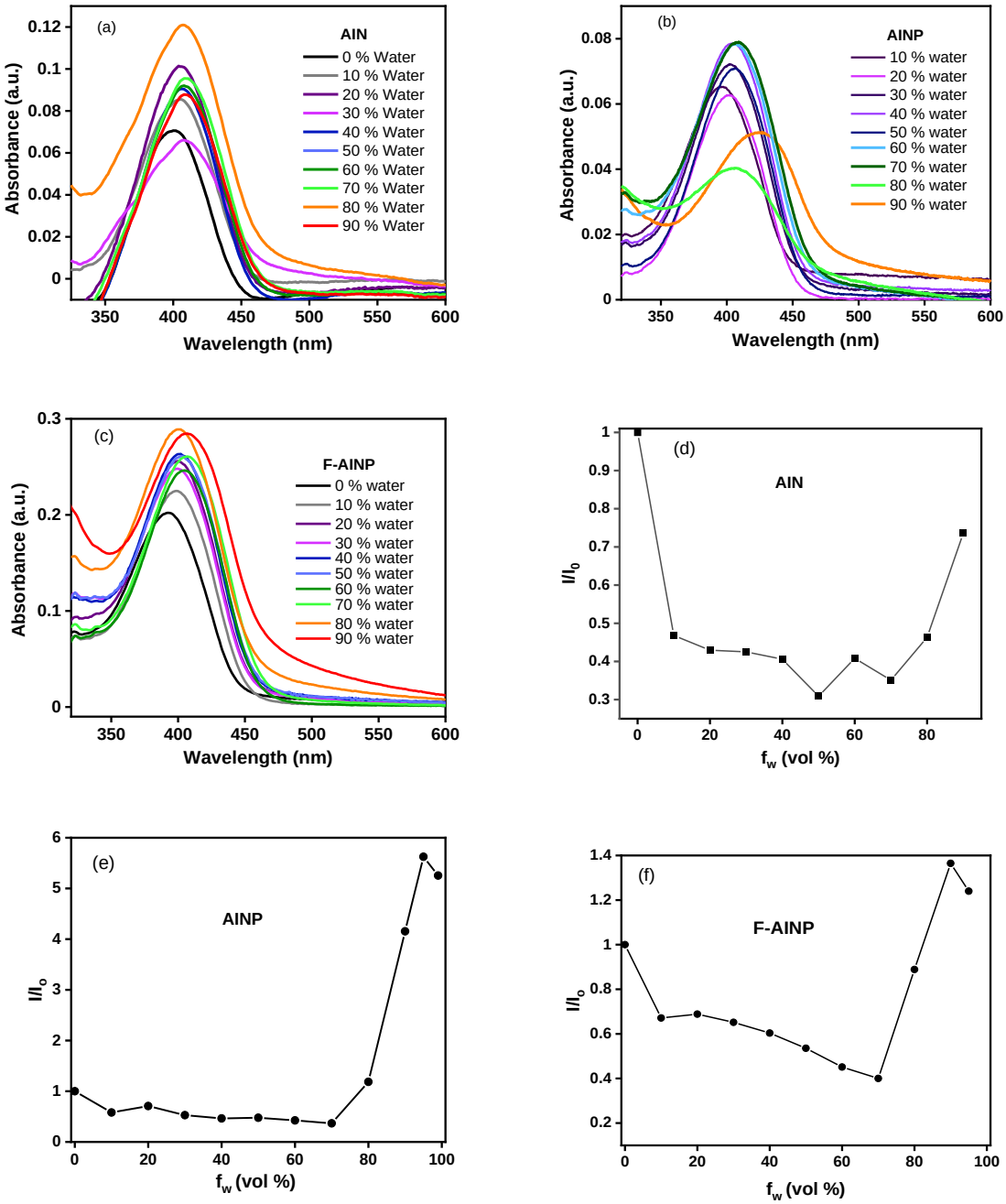

Figure S14. UV/Vis absorption of (a) **AIN**, (b) **AINP** and (c) **F-AINP** in different percentages of THF and water. The plot of I/I_0 versus f_w of (d) **AIN**, (e) **AINP** and (f) **F-AINP**. I_0 = Intensity at $f_w = 0$.

14. pH Sensing:

Addition of TBAF in Sample containing TFA:

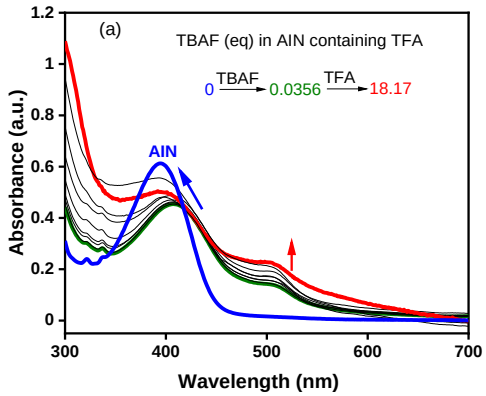

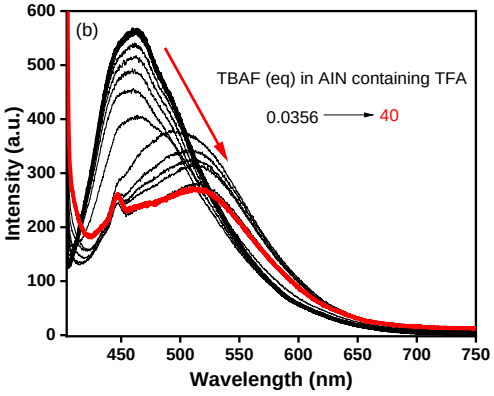

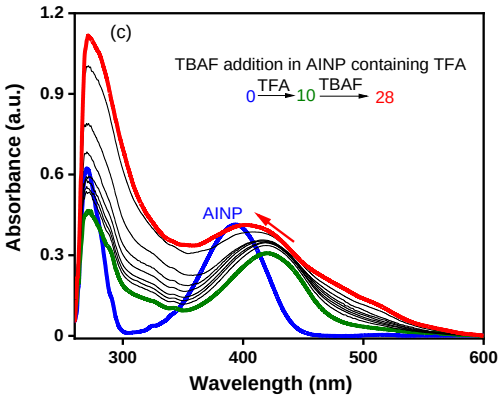

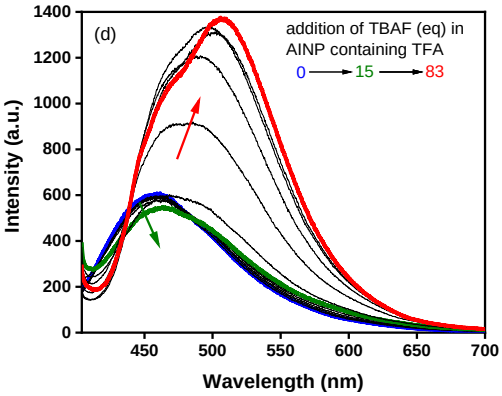

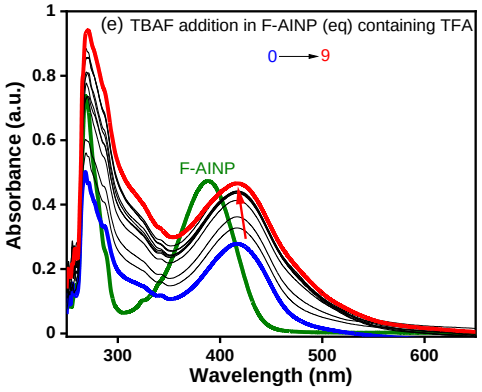

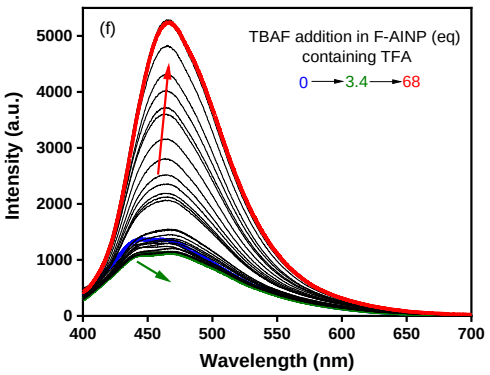

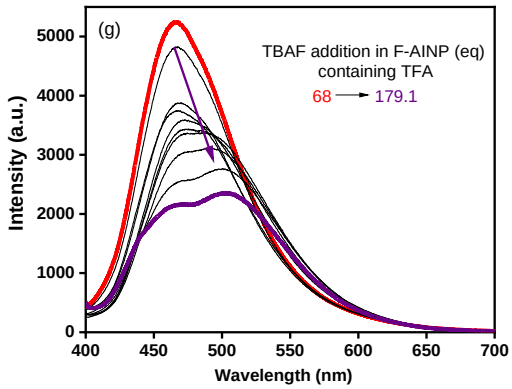

Figure S15. Absorption and emission of (a, b) **AIN,** (c, d) **AINP** and (e, f and g) **F-AINP** in $CHCl_3$ and TFA upon addition of TBAF respectively.

Addition of TFA in Sample containing TBAF:

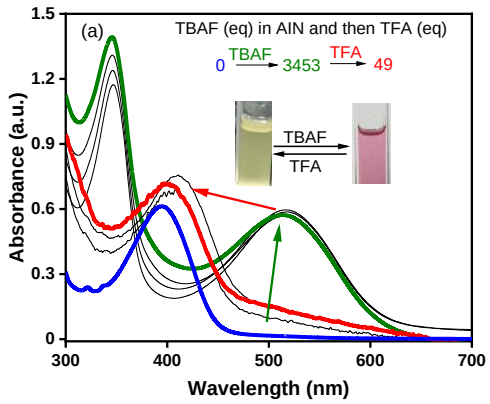

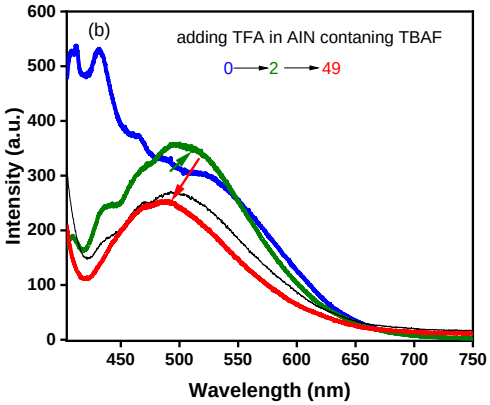

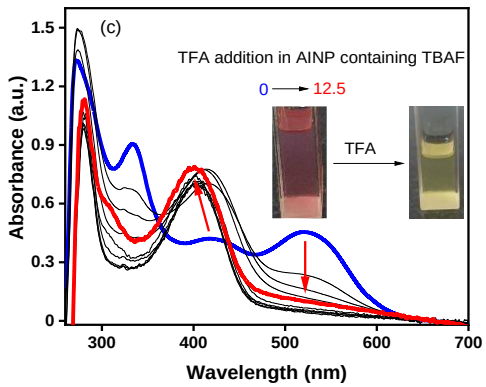

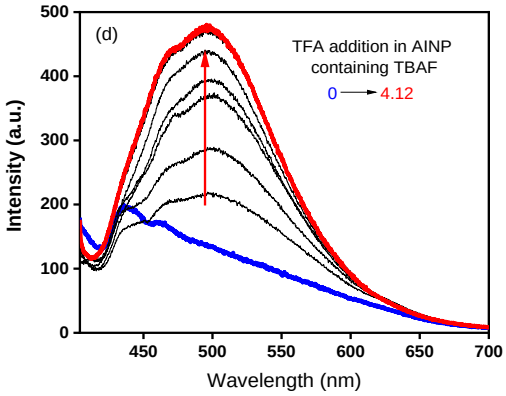

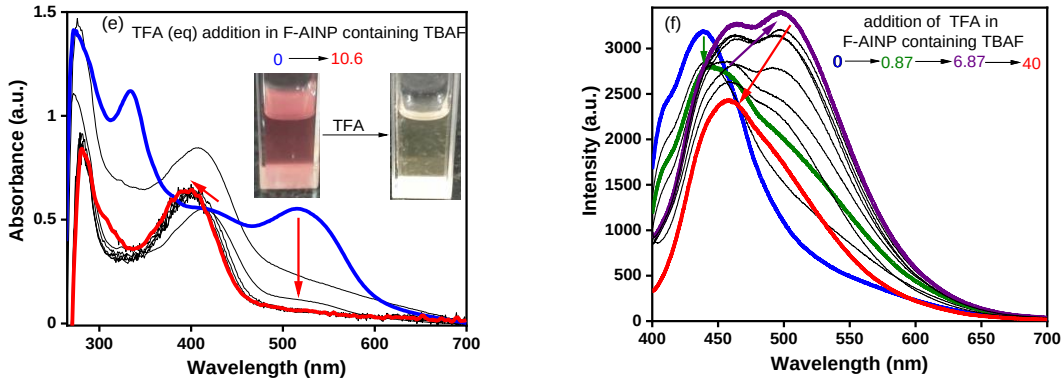

Figure S16. Absorption and emission of (a, b) **AIN,** (c, d) **AINP** and (e, f) **F-AINP** in $CHCl_3$ and TBAF upon addition of TFA respectively.

pH sensing in THF/Water Mixture:

The pH sensing of **AIN**, **AINP** and **F-AINP** were also performed in THF/water mixture (non-solubility of all compounds in water). Upon addition of HCl in solution of **AIN**, **AINP** and **F-AINP**, the absorbance decreases with a bathochromic shift of 29 nm, 47 nm and 30 nm respectively as shown in figure S17. While in case of emission spectra of **AIN**, the intensity first increases with the decrease in pH from 7 to 5.6 and then decreases with further decrease in pH from 5.6 to 1. Similarly, in case of **AINP** and **F-AINP**, the emission intensity first increases with the decrease in pH from 7 to 3.03 and from 7 to 6.24 and then decreases with further decrease in pH from 5.6 to 1 and 6.24 to 1.09 respectively as shown in figure S17. Figure S18 showed the absorbance vs pH graph and the calculated pKa values for **AIN**, **AINP** and **F-AINP** were observed to be 5.74, 3.36 and 3.63 respectively.[S9]

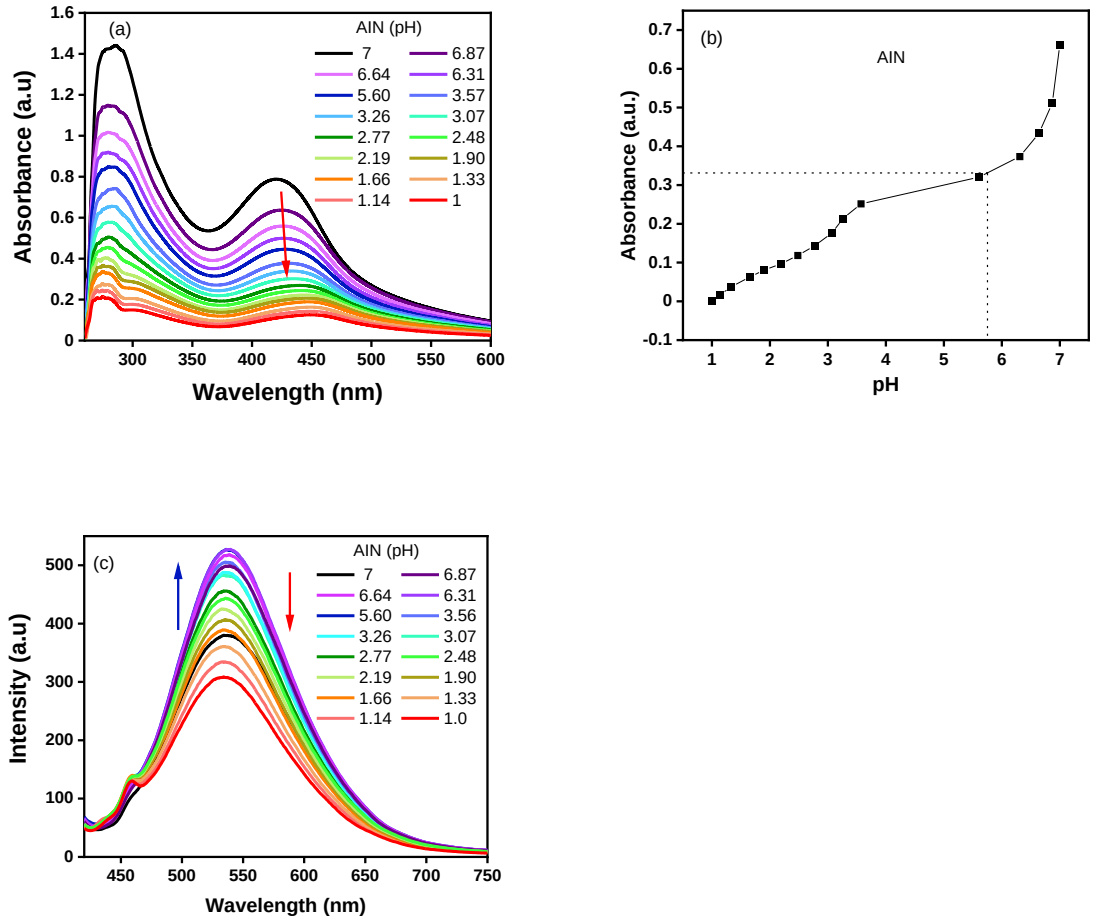

Figure S17. (a) Absorption, (b) plot of change in absorbance with the change in pH and (c) emission of **AIN** in THF/water mixture upon addition of HCl respectively.

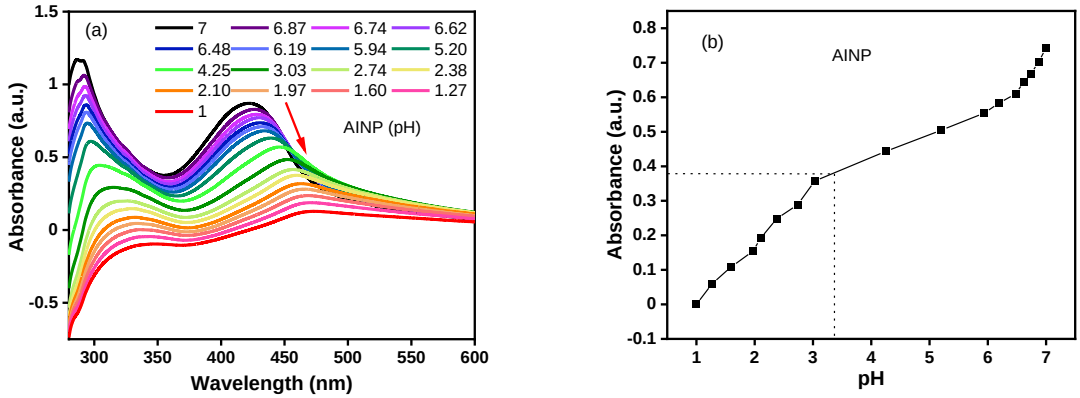

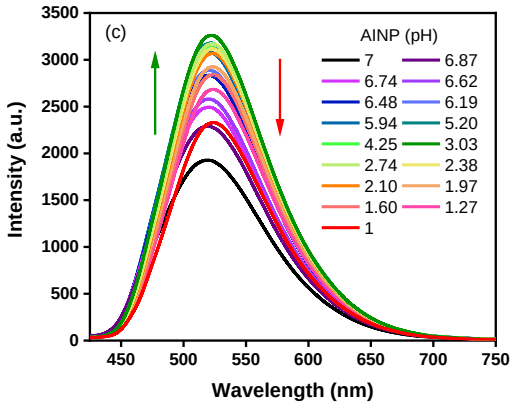

Figure S18. (a) Absorption, (b) plot of change in absorbance with the change in pH and (c) emission of **AINP** in THF/water mixture upon addition of HCl respectively.

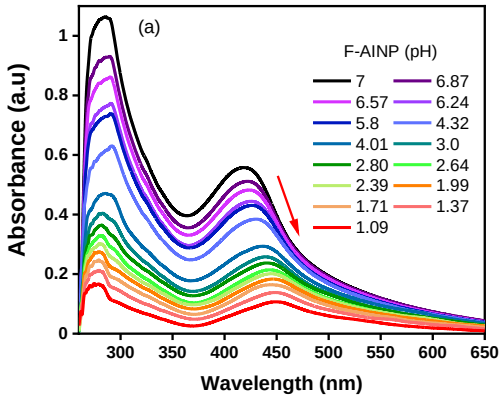

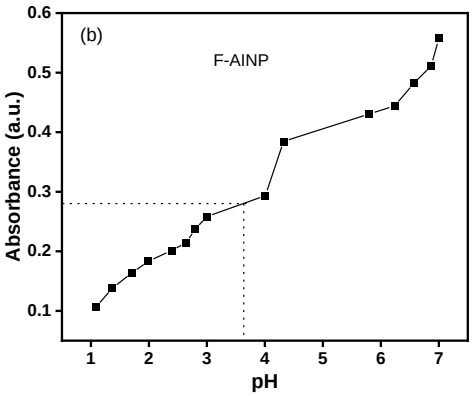

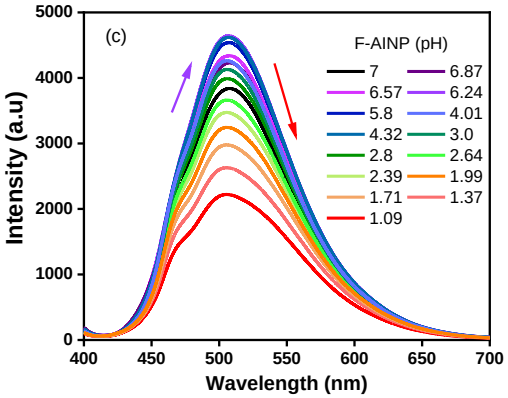

Figure S19. (a) Absorption, (b) plot of change in absorbance with the change in pH and (c) emission of **F-AINP** in THF/water mixture upon addition of HCl respectively.

15. Live Cell Imaging:

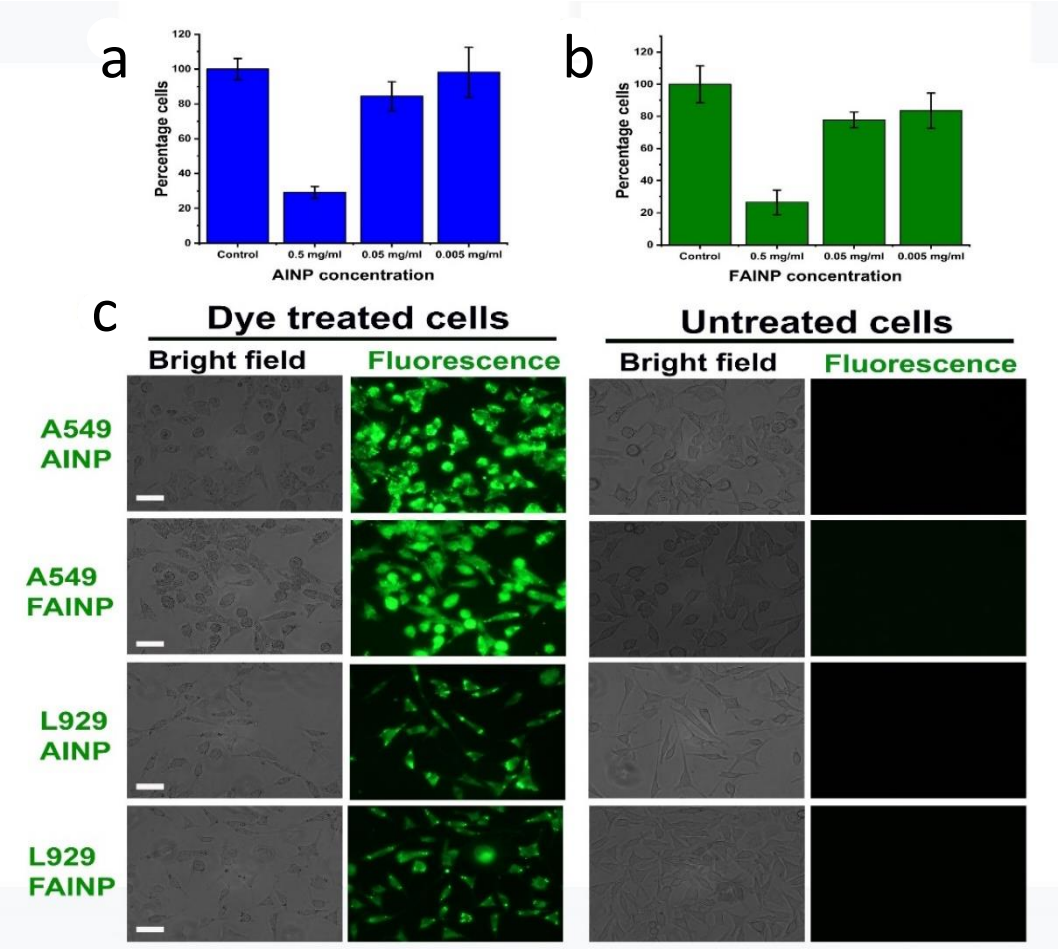

Figure S20. MTT assays were performed with A549 cells treated with **AINP** (**a**) and **F-AINP** (**b**), and the percentage of viable cells was plotted against dye concentration. Error bars represent the standard deviation measured for three independent experiments. (**c**) The representative bright field and fluorescence images of A549 and L929 cells treated and untreated (control) with **AINP** and **F-AINP**. Scale bar: 50 μm.

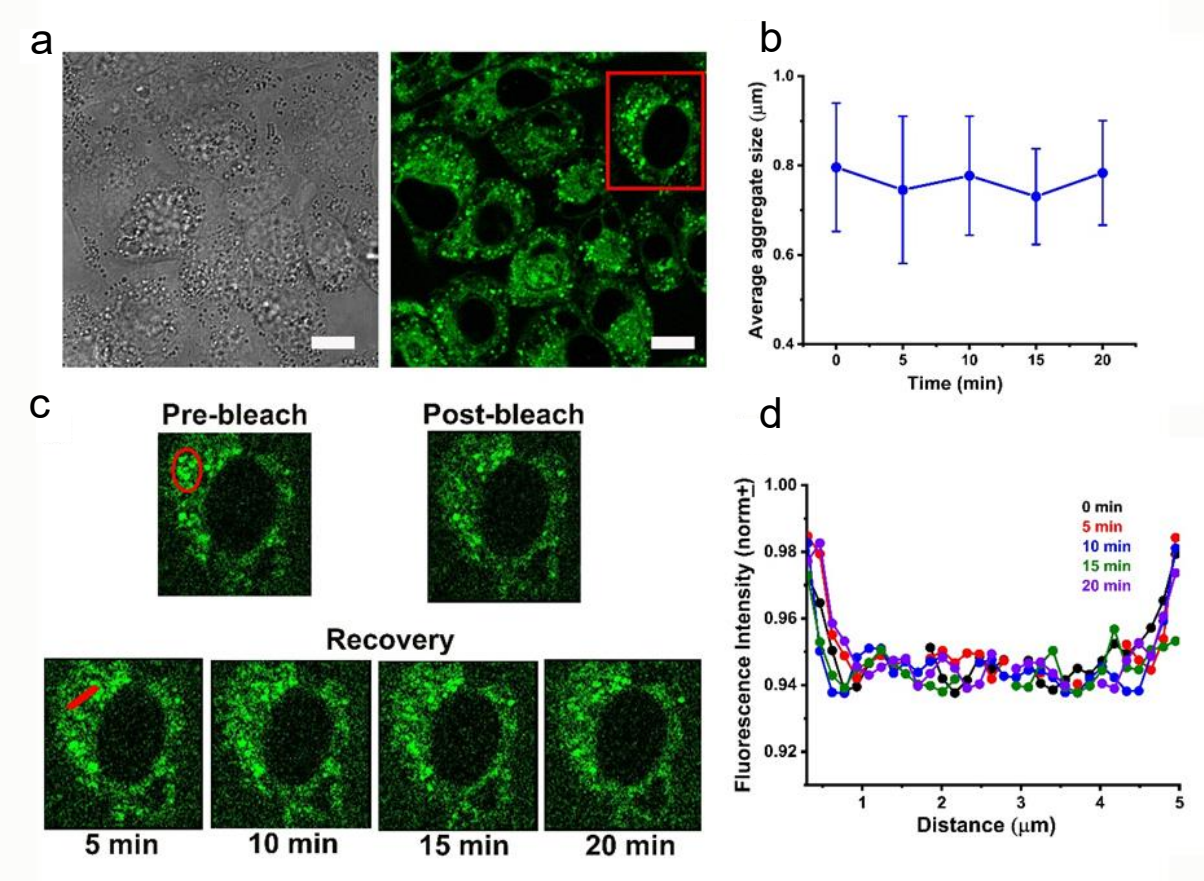

Figure S21. The dyes (AINP and F-AINP) induce the aggregates in the cellular environment. (a) The representative bright field and fluorescence images of A549 cells treated with **F-AINP** dye. The FRAP experiment is performed on the cell marked with a rectangle (red) in the fluorescence image. Scale bar: 10 μm. (b) The average aggregate size (μm) is plotted against time (min) for the A549 cell (marked in the rectangle (red)) treated with **F-AINP**. The error bars represent the standard deviation for n=15 aggregates. The average aggregate size did not change with time, which indicates that they are aggregates and do not have liquid-like characteristics. (c) The circle (red) indicates the confocal volume for the FRAP experiment. The cross-sections of fluorescence images indicate the regions of pre-bleach, bleach, and post-bleach recovery at the selected time points. The fluorescence recovery is monitored with time along the red line. The length of the line is 5 μm. No change in the fluorescence in the vicinity along the line indicates the nearby fluorescence spots are not mobile rather, they are aggregates. (d) The fluorescence intensity profile along the red line is plotted with the recovery time points.

16. Frequencies and Coordinates of DFT Optimized Geometries

Table S6: Results of first three frequencies and molecular symmetries calculated from geometry optimization of **AIN**, **AINP** and **F-AINP**.

Compounds	Symmetry	First Three Frequencies
AIN	C_1	23.76 26.11 33.92
AINP	C_1	12.84 15.47 21.10
F-AINP	C_1	13.66 16.13 20.84

Coordinates of geometry optimized structure of AIN

C	5.70056	1.12330	0.62647
C	4.80329	0.88924	1.68736
C	3.61432	0.19448	1.48813
C	3.35346	-0.26003	0.19373
C	4.24718	-0.05391	-0.88883
C	5.43420	0.66020	-0.65636
N	2.25302	-0.94694	-0.31012
C	2.48403	-1.24625	-1.65558
C	3.66770	-0.69116	-2.04443
N	1.32194	-1.58227	0.50052
C	-0.05362	-1.33671	0.35996
C	-0.90406	-2.43367	0.47663
C	-2.29393	-2.29613	0.40519
C	-2.86415	-1.05302	0.19266
C	-2.03306	0.09088	0.08314
C	-0.60825	-0.02089	0.18637
C	-2.62320	1.36779	-0.10595
C	-1.84056	2.50685	-0.16825
C	-0.44566	2.40507	-0.03000
C	0.15771	1.17452	0.14262
C	-4.32683	-0.93421	0.08764
O	-4.84322	0.33851	-0.12777
C	-4.09176	1.49776	-0.22913
O	-4.67695	2.53672	-0.40973
O	-5.10754	-1.85029	0.17078
H	6.61697	1.67284	0.81884
H	5.04395	1.25724	2.68007
H	2.91863	0.00435	2.29845
H	6.13412	0.84088	-1.46700
H	1.74536	-1.80250	-2.21457
H	4.08151	-0.71911	-3.04253
H	1.53874	-2.56549	0.63135
H	-0.47447	-3.42342	0.60788
H	-2.94172	-3.16180	0.48960
H	-2.32650	3.46575	-0.31187
H	0.16499	3.30163	-0.05505

H	1.23121	1.13002	0.25748

Coordinates of geometry optimized structure of AIN^{+}

C	-6.45273	-0.10509	0.15388
C	-5.82324	0.70160	1.11488
C	-4.44864	0.94327	1.06658
C	-3.73924	0.32939	0.03927
C	-4.34509	-0.50449	-0.92146
C	-5.72870	-0.70669	-0.87357
N	-2.36022	0.44145	-0.30680
C	-2.11245	-0.47370	-1.37301
C	-3.29066	-0.98519	-1.79755
N	-1.44194	0.37169	0.83315
C	-0.02044	0.63420	0.50572
C	0.33164	1.94032	0.24467
C	1.67358	2.24876	-0.04259
C	2.61968	1.24143	-0.05374
C	2.25957	-0.10380	0.20567
C	0.89729	-0.45056	0.48475
C	3.24975	-1.11879	0.18522
C	2.91100	-2.43509	0.42712
C	1.56773	-2.78085	0.68855
C	0.58151	-1.81737	0.71572
C	4.04045	1.59202	-0.34664
O	4.95629	0.56277	-0.34577
C	4.66790	-0.77274	-0.10032
O	5.56364	-1.56929	-0.13102
O	4.41231	2.70986	-0.57805
H	-7.52505	-0.25797	0.21301
H	-6.41440	1.15877	1.90095
H	-3.98618	1.60233	1.79788
H	-6.22520	-1.32159	-1.61692
H	-1.11888	-0.55869	-1.78622
H	-3.42268	-1.61082	-2.66981
H	-0.41655	2.72761	0.25329
H	1.98032	3.26774	-0.24892
H	3.68890	-3.19046	0.40653
H	1.30874	-3.81923	0.86510
H	-0.44229	-2.13837	0.89215
H	-1.76468	1.09351	1.48635
H	-1.53810	-0.53142	1.32202

Coordinates of geometry optimized structure of AIN^{-}

C	-6.07476	0.27980	-1.31249
C	-5.00364	1.05517	-1.81091
C	-3.75556	1.03392	-1.20178
C	-3.59960	0.21905	-0.07430
C	-4.66923	-0.56457	0.45830
C	-5.91688	-0.52476	-0.19102
N	-2.48724	0.00439	0.70641
C	-2.83070	-0.85314	1.73189
C	-4.14788	-1.23683	1.60989
N	-1.31376	0.77243	0.60905
C	-0.21203	0.07476	0.35422
C	-0.10893	-1.33442	0.10167
C	1.10237	-1.93511	-0.16003
C	2.31781	-1.22067	-0.18683
C	2.28153	0.17940	0.05160
C	1.04637	0.84247	0.32041
C	3.47829	0.94251	0.02471

C	3.45574	2.31550	0.25611
C	2.24482	2.95974	0.52266
C	1.06117	2.22624	0.55539
C	3.55933	-1.89265	-0.45634
O	4.72545	-1.08203	-0.47155
C	4.75994	0.27392	-0.25095
O	5.84066	0.83188	-0.29653
O	3.73931	-3.07627	-0.67466
H	-7.03724	0.31620	-1.81702
H	-5.15989	1.67738	-2.68851
H	-2.92075	1.62121	-1.56841
H	-6.74909	-1.11630	0.18446
H	-2.08889	-1.11640	2.47161
H	-4.67503	-1.91578	2.26611
H	-1.01464	-1.92862	0.09482
H	1.14637	-3.00184	-0.36229
H	4.39562	2.85735	0.22524
H	2.22582	4.03015	0.70796
H	0.11251	2.70822	0.76656

Coordinates of geometry optimized structure of AINP

C	-0.16453	-1.60072	2.07236
C	1.19722	-1.93675	1.98111
C	1.92217	-1.63860	0.84452
C	1.31676	-0.98640	-0.26289
C	-0.07924	-0.66851	-0.17472
C	-0.79618	-0.98009	1.01027
C	2.00360	-0.64369	-1.47840
C	1.29857	-0.06079	-2.52702
C	-0.06933	0.21717	-2.42724
C	-0.76018	-0.06650	-1.26319
N	3.35788	-0.95445	-1.72009
C	-2.19892	0.26781	-1.18307
N	-2.85447	-0.04718	0.02474
C	-2.24212	-0.65797	1.13429
O	-2.88474	-0.90908	2.14302
O	-2.80801	0.79462	-2.10312
N	4.32846	-0.73703	-0.75128
C	5.20847	-1.72734	-0.32915
C	6.13121	-1.18111	0.51727
C	5.83911	0.22485	0.62069
C	4.70896	0.48267	-0.20115
C	6.42434	1.29535	1.31789
C	5.88708	2.56778	1.17360
C	4.77007	2.79738	0.34559
C	4.16206	1.75999	-0.35298
H	-0.74575	-1.82366	2.96043
H	1.68512	-2.43664	2.81171
H	2.96710	-1.91160	0.80380
H	1.82718	0.19539	-3.44187
H	-0.60513	0.67751	-3.25011
C	-4.26558	0.27740	0.12882
H	3.66602	-0.61471	-2.62681
C	-4.63330	1.57795	0.50166
C	-5.99790	1.87047	0.59686
C	-6.95794	0.89781	0.32885
C	-6.56524	-0.38649	-0.03993
C	-5.21108	-0.72045	-0.14680
C	-3.59507	2.63513	0.78441
H	-6.30427	2.87243	0.88422

H	5.07459	-2.73767	-0.68640
H	6.93093	-1.71386	1.01154
H	7.28687	1.12714	1.95638
H	6.33259	3.40254	1.70610
H	4.37339	3.80374	0.25251
H	3.29676	1.93614	-0.98284
H	-8.01364	1.14102	0.40742
H	-7.31421	-1.14524	-0.24900
C	-4.78772	-2.11423	-0.53865
H	-2.89700	2.31501	1.56524
H	-3.00920	2.86060	-0.11324
H	-4.06876	3.56179	1.11774
H	-5.65897	-2.73017	-0.77473
H	-4.13526	-2.10386	-1.41822
H	-4.24115	-2.60240	0.27546

Coordinates of geometry optimized structure of AINP^{+}

C	-0.61421	2.61572	0.85120
C	0.78012	2.81881	0.77604
C	1.60872	1.86043	0.22926
C	1.06334	0.65195	-0.27829
C	-0.35055	0.44227	-0.19227
C	-1.17270	1.44394	0.37964
C	1.80392	-0.39435	-0.88988
C	1.23641	-1.55856	-1.35976
C	-0.15467	-1.74323	-1.24679
C	-0.93350	-0.75555	-0.67637
N	3.26154	-0.22388	-1.07716
C	-2.41402	-0.98061	-0.58312
N	-3.17588	0.04212	-0.00983
C	-2.65203	1.25220	0.48161
O	-3.36992	2.10454	0.96820
O	-2.91390	-2.01243	-0.99268
N	4.06286	-0.28840	0.14546
C	3.96532	-1.48787	0.90767
C	5.19803	-1.83035	1.34821
C	6.16522	-0.91450	0.76966
C	5.44714	-0.00146	-0.02878
C	7.55670	-0.79533	0.85728
C	8.18692	0.20118	0.11492
C	7.45283	1.08237	-0.69456
C	6.06089	1.00223	-0.77198
C	-4.61691	-0.15916	0.08624
C	-5.42240	0.25166	-0.98456
C	-6.80152	0.04892	-0.87031
C	-7.34569	-0.53970	0.26870
C	-6.51791	-0.93664	1.31615
C	-5.13313	-0.75359	1.24570
C	-4.83395	0.89034	-2.21858
C	-4.23734	-1.18151	2.38211
H	-1.26828	3.36545	1.28272
H	1.20645	3.73801	1.16367
H	2.68109	2.02822	0.22742
H	1.84708	-2.33093	-1.82090
H	-0.63243	-2.64679	-1.60749
H	3.60025	-0.91628	-1.76335
H	3.44423	0.70514	-1.47560
H	2.99432	-1.89786	1.14015
H	5.41344	-2.62921	2.04454
H	8.13181	-1.46831	1.48465

H	9.26596	0.30210	0.16254
H	7.97192	1.84798	-1.26101
H	5.50826	1.71513	-1.37976
H	-7.44992	0.35800	-1.68465
H	-8.41856	-0.68905	0.34053
H	-6.94561	-1.39442	2.20306
H	-4.29584	1.81360	-1.97640
H	-4.13440	0.21638	-2.72583
H	-5.62115	1.14502	-2.93131
H	-4.82531	-1.62705	3.18729
H	-3.50288	-1.92721	2.05755
H	-3.68971	-0.33136	2.80405

Coordinates of geometry optimized structure of AINP$^-$

C	-1.18788	3.15870	-0.34135
C	0.12941	3.61962	-0.28528
C	1.16910	2.72208	-0.05405
C	0.92991	1.35044	0.11987
C	-0.41618	0.87380	0.06589
C	-1.46405	1.80447	-0.16714
C	2.03915	0.40919	0.36071
C	1.68266	-0.97082	0.52499
C	0.37269	-1.39041	0.45807
C	-0.70347	-0.50608	0.23958
N	3.25799	0.93897	0.39325
C	-2.05531	-1.00600	0.18456
N	-3.08086	-0.02573	-0.04856
C	-2.86599	1.35086	-0.22482
O	-3.81578	2.11432	-0.40967
O	-2.39010	-2.18692	0.31454
N	4.28647	0.02978	0.69660
C	4.54031	-0.55217	1.92189
C	5.76205	-1.18811	1.90278
C	6.31889	-0.97401	0.60134
C	5.36862	-0.19082	-0.12376
C	7.51224	-1.34656	-0.04441
C	7.73612	-0.93320	-1.35172
C	6.78517	-0.14791	-2.04166
C	5.59215	0.23101	-1.43970
C	-4.44478	-0.49790	-0.10028
C	-4.90197	-1.14896	-1.25727
C	-6.22728	-1.59645	-1.28916
C	-7.07536	-1.40328	-0.20147
C	-6.60227	-0.75683	0.93770
C	-5.28323	-0.29527	1.00754
C	-3.98529	-1.37960	-2.43161
C	-4.78294	0.41432	2.24023
H	-2.02192	3.83063	-0.51648
H	0.34339	4.67677	-0.41726
H	2.19792	3.06192	-0.00051
H	2.47139	-1.69708	0.68004
H	0.13214	-2.44407	0.57008
H	3.81121	-0.45705	2.71319
H	6.20428	-1.73903	2.72159
H	8.25228	-1.94969	0.47725
H	8.65750	-1.21631	-1.85492
H	6.99127	0.16271	-3.06285
H	4.84947	0.83338	-1.95137
H	-6.59138	-2.10240	-2.18010
H	-8.10264	-1.75687	-0.24112

H	-7.25994	-0.60489	1.79020
H	-3.49395	-0.45290	-2.74497
H	-3.19912	-2.09172	-2.16102
H	-4.53953	-1.77974	-3.28573
H	-5.51917	0.35771	3.04743
H	-3.84549	-0.02202	2.59935
H	-4.59067	1.46966	2.02031

Coordinates of geometry optimized structure of F-AINP

C	-0.31200	-2.00000	1.75405
C	1.04820	-2.32042	1.60498
C	1.77893	-1.81839	0.54662
C	1.18322	-0.96579	-0.42180
C	-0.21192	-0.66050	-0.27691
C	-0.93513	-1.18627	0.82609
C	1.87391	-0.40228	-1.54895
C	1.17698	0.37730	-2.46523
C	-0.18802	0.64125	-2.31664
C	-0.88553	0.14234	-1.23127
N	3.22416	-0.67329	-1.85911
C	-2.32249	0.46346	-1.09344
N	-2.98522	-0.07221	0.03044
C	-2.37987	-0.88489	1.00555
O	-3.02695	-1.31931	1.94716
O	-2.92584	1.15887	-1.89801
N	4.20704	-0.69881	-0.87770
C	5.00649	-1.81083	-0.64692
C	5.93000	-1.51865	0.31657
C	5.72748	-0.14884	0.70781
C	4.64749	0.34499	-0.07225
C	6.36116	0.70375	1.63075
C	5.92004	2.01338	1.74887
C	4.85814	2.50405	0.96133
C	4.23033	1.67109	0.05575
C	-4.39536	0.23343	0.18900
C	-4.76004	1.44911	0.78486
C	-6.12397	1.72464	0.92846
C	-7.08648	0.81764	0.49207
C	-6.69692	-0.38278	-0.09685
C	-5.34357	-0.69704	-0.25938
C	-3.71962	2.43752	1.24956
F	3.22061	2.13744	-0.71758
C	-4.92432	-2.00183	-0.88957
H	-0.89828	-2.38269	2.58227
H	1.53079	-2.97014	2.32810
H	2.82181	-2.08806	0.46175
H	1.71176	0.80778	-3.30770
H	-0.71714	1.25683	-3.03571
H	3.53533	-0.14164	-2.66598
H	4.81951	-2.71428	-1.20807
H	6.67665	-2.19571	0.70557
H	7.18474	0.33906	2.23644
H	6.39897	2.68373	2.45535
H	4.52016	3.53079	1.04690
H	-6.42777	2.66130	1.38755
H	-8.14160	1.04667	0.61095
H	-7.44773	-1.09039	-0.43740
H	-3.01561	1.98059	1.95310
H	-3.14048	2.82398	0.40396
H	-4.19072	3.28683	1.75051

H	-5.79657	-2.55847	-1.24110
H	-4.26101	-1.84045	-1.74593
H	-4.39066	-2.63161	-0.16956

Coordinates of geometry optimized structure of F-AINP^{+}

C	-0.67276	2.49775	0.95029
C	0.72399	2.67002	0.84766
C	1.51522	1.71583	0.24198
C	0.92709	0.54169	-0.29757
C	-0.49074	0.36915	-0.19701
C	-1.27341	1.36532	0.43653
C	1.62757	-0.50155	-0.95940
C	1.01729	-1.62163	-1.48061
C	-0.37825	-1.76489	-1.36393
C	-1.11724	-0.78489	-0.73059
N	3.09251	-0.38960	-1.11183
C	-2.60247	-0.96942	-0.62563
N	-3.32370	0.04408	0.01280
C	-2.75531	1.21087	0.55742
O	-3.43924	2.05548	1.10294
O	-3.14042	-1.96222	-1.08118
N	3.85264	-0.65987	0.10816
C	3.85117	-1.98053	0.63302
C	5.09229	-2.27213	1.09585
C	5.98054	-1.16838	0.77073
C	5.19067	-0.21666	0.10119
C	7.33920	-0.89317	0.98062
C	7.86457	0.29859	0.48370
C	7.07216	1.23516	-0.20792
C	5.72849	0.96461	-0.38077
C	-4.76848	-0.11868	0.12228
C	-5.57508	0.34614	-0.92542
C	-6.95799	0.17969	-0.79882
C	-7.50487	-0.42618	0.32978
C	-6.67600	-0.87706	1.35427
C	-5.28748	-0.73171	1.27080
C	-4.98374	1.00184	-2.14907
F	4.88579	1.82502	-1.03863
C	-4.39071	-1.21644	2.38335
H	-1.29678	3.24448	1.42891
H	1.18190	3.56523	1.25482
H	2.58704	1.87714	0.19003
H	1.59823	-2.39069	-1.98403
H	-0.89002	-2.63197	-1.76521
H	3.40610	-1.00922	-1.87394
H	3.36231	0.57251	-1.37405
H	2.92308	-2.52659	0.71150
H	5.35834	-3.16271	1.64828
H	7.97186	-1.59320	1.51504
H	8.91614	0.52005	0.62976
H	7.49159	2.15695	-0.59430
H	-7.60717	0.53087	-1.59528
H	-8.58066	-0.54680	0.41145
H	-7.10573	-1.34811	2.23324
H	-4.40165	1.89265	-1.88801
H	-4.32381	0.31619	-2.69247
H	-5.77289	1.31352	-2.83655
H	-4.98021	-1.68129	3.17643
H	-3.67086	-1.96154	2.02635
H	-3.82614	-0.39102	2.83127

Coordinates of geometry optimized structure of F-AINP$^-$

C	-1.38477	3.24299	-0.11656
C	-0.09108	3.76182	-0.02034
C	0.98536	2.90515	0.19474
C	0.80584	1.51901	0.32036
C	-0.51452	0.98273	0.22008
C	-1.60051	1.87213	0.00091
C	1.95059	0.62297	0.55521
C	1.66005	-0.77645	0.65387
C	0.37222	-1.25466	0.55043
C	-0.73918	-0.41435	0.33815
N	3.14102	1.20609	0.66345
C	-2.06660	-0.97293	0.24764
N	-3.13152	-0.03413	0.02128
C	-2.97737	1.35573	-0.10981
O	-3.95572	2.07782	-0.31031
O	-2.35078	-2.16908	0.35366
N	4.19543	0.29706	0.89799
C	4.72547	0.04226	2.13943
C	5.87090	-0.71640	2.02925
C	6.08662	-0.93892	0.63395
C	5.01626	-0.27641	-0.04717
C	7.06859	-1.62062	-0.11366
C	6.98165	-1.62932	-1.49679
C	5.92618	-0.97097	-2.16750
C	4.95436	-0.30346	-1.44621
C	-4.46954	-0.56737	-0.08415
C	-5.05950	-0.69324	-1.35199
C	-6.35774	-1.20877	-1.43394
C	-7.05074	-1.58984	-0.28768
C	-6.44723	-1.45893	0.96065
C	-5.15068	-0.94754	1.08332
C	-4.32127	-0.27153	-2.59718
F	3.94758	0.31705	-2.09928
C	-4.49764	-0.82710	2.43670
H	-2.24573	3.88195	-0.28482
H	0.07576	4.83135	-0.11524
H	1.99744	3.28825	0.27005
H	2.47920	-1.46636	0.81888
H	0.17829	-2.32043	0.63418
H	4.22357	0.44048	3.00914
H	6.48247	-1.07155	2.84695
H	7.88358	-2.13120	0.39296
H	7.73237	-2.15011	-2.08509
H	5.85405	-0.97872	-3.25002
H	-6.82386	-1.31058	-2.41104
H	-8.05874	-1.98925	-0.36709
H	-6.98347	-1.75698	1.85841
H	-4.19518	0.81607	-2.61529
H	-3.32286	-0.71797	-2.64034
H	-4.87011	-0.57085	-3.49492
H	-5.21277	-1.04617	3.23513
H	-3.66131	-1.52913	2.51483
H	-4.09765	0.17865	2.60077

14. References

S1 Gaussian 09, Revision C.01, M. J. Frisch, G. W. Trucks, H. B. Schlegel, G. E. Scuseria, M. A. Robb, J. R. Cheeseman, G. Scalmani, V. Barone, B. Mennucci, G. A. Petersson, H. Nakatsuji, M. Caricato, X. Li, H. P. Hratchian, A. F. Izmaylov, J. Bloino, G. Zheng, J. L. Sonnenberg, M. Hada, M. Ehara, K. Toyota, R. Fukuda, J. Hasegawa, M. Ishida, T. Nakajima, Y. Honda, O. Kitao, H. Nakai, T. Vreven, J. A. Montgomery, Jr., J. E. Peralta, F. Ogliaro, M. Bearpark, J. J. Heyd, E. Brothers, K. N. Kudin, V. N. Staroverov, T. Keith, R. Kobayashi, J. Normand, K. Raghavachari, A. Rendell, J. C. Burant, S. S. Iyengar, J. Tomasi, M. Cossi, N. Rega, J. M. Millam, M. Klene, J. E. Knox, J. B. Cross, V. Bakken, C. Adamo, J. Jaramillo, R. Gomperts, R. E. Stratmann, O. Yazyev, A. J. Austin, R. Cammi, C. Pomelli, J. W. Ochterski, R. L. Martin, K. Morokuma, V. G. Zakrzewski, G. A. Voth, P. Salvador, J. J. Dannenberg, S. Dapprich, A. D. Daniels, O. Farkas, J. B. Foresman, J. V. Ortiz, J. Cioslowski, and D. J. Fox, Gaussian, Inc., Wallingford CT, 2010.

S2 M. Somei, M. Matsubara, Y. Kanda, and M. Natsume, *Chem. Pharm. Bull*, 1978, **26**, 2522-2534.

S3 A. R. Mallia, A. M. Philip, V. Bhat, and M. Hariharan, *J. Phys. Chem. C*, 2017, **121**, 4765-4777.

S4 T. T. H. Luong, J. D. Brion, M. Alami, and S. Messaoudi, *J. Org. Chem.*, 2015, **80**, 751-761.

S5 F. Liu, T. Wu, J. Cao, S. Cui, Z. Yang, X. Qiang, S. Sun, F. Song, J. Fan, J. Wang and X. Peng, *Chem. Eur. J.*, 2013, **19**, 1548–1553.

S6 S. K. Mishra and N. Suryaprakash, *Molecules*, 2017, **22**, 423.

S7 G. Chen, H. Sasabe, Y. Sasaki, H. Katagiri, X. F. Wang, T. Sano, Z. Hong, Y. Yang, and J. Kido, *Chem. Mater.*, 2014, **26**,1356-1364.

S8 B. Sk, S. Khodia and A. Patra, *Chem. Commun*., 2018, **54**, 1786–1789.

S9 A. A. Shalaby and A. A. Mohamed, *RSC Adv*., 2020, **10**, 11311–11316.